OLD DOMINION UNIVERSITY RESEARCH FOUNDATION

DEPARTMENT OF MECHANICAL ENGINEERING AND MECHANICS
SCHOOL OF ENGINEERING
OLD DOMINION UNIVERSITY
NORFOLK, VIRGINIA 23508

ADAPTIVE CONTROL OF LARGE SPACE STRUCTURES USING RECURSIVE LATTICE FILTERS

By

Gene L. Goglia, Principal Investigator

Final Report
For the period ending December 31, 1985

Prepared for the
National Aeronautics and Space Administration
Langley Research Center
Hampton, Virginia 23665

Under
Research Grant NAG-1-429
Dr. Raymond C. Montgomery, Technical Monitor
FDCD-Spacecraft Controls Branch

December 1985

DEPARTMENT OF MECHANICAL ENGINEERING AND MECHANICS
SCHOOL OF ENGINEERING
OLD DOMINION UNIVERSITY
NORFOLK, VIRGINIA 23508

ADAPTIVE CONTROL OF LARGE SPACE STRUCTURES USING RECURSIVE LATTICE FILTERS

By

Gene L. Goglia, Principal Investigator

Final Report
For the period ending December 31, 1985

Prepared for the
National Aeronautics and Space Administration
Langley Research Center
Hampton, Virginia 23665

Under
Research Grant NAG-1-429
Dr. Raymond C. Montgomery, Technical Monitor
FDCD-Spacecraft Controls Branch

Submitted by the
Old Dominion University Research Foundation
P.O. Box 6369
Norfolk, Virginia 23508

December 1985

TABLE OF CONTENTS

ADAPTIVE CONTROL OF LARGE SPACE STRUCTURES USING RECURSIVE LATTICE FILTERS

By

Gene L. Goglia*

SUMMARY

This report summarizes the research activities performed under grant NAG-1-429. The objective of the research has been to study the use of recursive lattice filters for identification and adaptive control of large space structures. Lattice filters are used widely in the areas of speech and signal processing. Herein, they are used to identify the structural dynamics model of the flexible structures. This identified model is then used for adaptive control. Before the identified model and control laws are integrated, the identified model is passed through a series of validation procedures and only when the model passes these validation procedures control is engaged. This type of validation scheme prevents instability when the overall loop is closed.

One of the main aims of the research has been to compare the results obtained from simulation to those obtained from experiments. In this regard, the flexible beam and grid apparatus at the Aerospace Control Research Lab (ACRL) of NASA Langley Research Center were used as the principal candidates for carrying out the above tasks. Another important area of research namely that of robust controller synthesis was investigated using frequency domain multivariable controller synthesis methods. The method uses the Linear Quadratic Gaussian/Loop Transfer Recovery (LQG/LTR) approach to ensure stability against unmodeled higher frequency modes and achieves the

*Eminent Professor, Department of Mechanical Engineering and Mechanics, Old Dominion University, Norfolk, Virginia 23508.

desired performance. Such a controller was designed for the 122 mr. Hoop-Column antenna using a single 3-axis torque actuator and attitude sensors.

References 1 and 2 present the detailed analysis of identification results for the flexible grid apparatus using lattice filters. The scheme provides on-line identification of number of modes, mode shapes, modal damping and natural frequencies. The results indicate that the lattice identification scheme is a viable scheme for identifying the structural dynamics of flexible structures. The experimental results also indicate differences between those predicted by finite element analysis and obtained by experiments. The difficulties are not as such in finite element analysis but in modeling the apparatus for finite element analysis. This fact emphasises the need for on-orbit identification of large space structures before control is attempted. A summary of the experimental results obtained using lattice filters is described in reference 3.

An adaptive control scheme using lattice filter identification and modal description has been developed in reference 4. Alternate schemes of using input-output models instead of modal form from lattice filters is described therein. The problem in this approach is to obtain efficient control schemes as the identified model of the system becomes coupled and to calculate the pole placement control law on-line is computationally complex. Presently, the identification scheme using lattice filters for obtaining the input-output model is under development in the Charles River Data Systems in the ACRL.

A new approach of designing robust controller for a large flexible space antenna using the LQG/LTR approach was developed in reference 5. The method was used in designing robust controller for the 122 mr. Hoop-Column antenna using only a 3 axis torque actuator and attitude sensor. The objec-

tive is to design the controller based on a lower order model to achieve the desired bandwidth and at the same time ensuring stability against unmodeled higher frequency modes. The results in reference 5 indicated that if one uses only a rigid body model for design stability against unmodeled modes can be obtained but not the performance. Based on detailed studies in references 6 and 7 it was concluded that with the first three flexible modes (corresponding to the 3 axes) included in the design model both stability and performance can be ensured.

REFERENCES

1. R. C. Montgomery and N. Sundararajan, "Identification of the Dynamics of a Two-Dimensional Grid Structure Using Least Square Lattice Filters," Proc. of American Control Conference, San Diego, June 1984, pp. 704-709.

   Also, appears in J. of Astronautical Sciences, Vol. 33, No. 1, January-March, 1985, pp. 35-47.

2. N. Sundararajan, "Experimental Evaluation of Flexible Structure Identification Using Lattice Filters," Proc. of 7th IFAC Symposium on Identification and System Parameter Estimation, York, England, July, 1985, pp. 687-692.

3. N. Sundararajan and R. C. Montgomery, "Progress in Adaptive Control of Flexible Spacecraft Using Lattice Filters," Proc. of Workshop on Applications of Adaptive Control, Yale University, New Haven, CT, May 1985, pp. 162-167.

   Also, to appear in a book on "Adaptive and Learning Systems: Theory and Applications," Ed. Prof. K. S. Narendra, Plenum Press.

4. N. Sundararajan, S. M. Joshi, and E. S. Armstrong, "Robust Controller Synthesis for a Large Flexible Antenna," Proc. of 23 IEEE Conference on Decision and Control, Las Vegas, Nevada, Dec. 1984, pp.

   Also, revised version has been submitted for publication in AIAA J. on Guidance, Control and Dynamics.

5. N. Sundararajan, S. M. Joshi, and E. S. Armstrong, "Application of the LQG/LTR Technique to Robust Controller Synthesis for a Large Flexible Space Antenna." To appear as a NASA - Technical Paper (TP).

APPENDIX A

IDENTIFICATION OF THE DYNAMICS OF A TWO-DIMENSIONAL GRID STRUCTURE USING LEAST SQUARES LATTICE FILTERS

The Journal of the Astronautical Sciences, Vol. 33, No. 1, January-March 1985, pp. 35-47

Identification of the Dynamics of a Two-Dimensional Grid Structure using Least Squares Lattice Filters[1]

R. C. Montgomery[2] and N. Sundararajan[3]

Abstract

The basic theory of least squares lattice filters and their use in identification of structural dynamics systems is summarized. Thereafter, this theory is applied to a two-dimensional grid structure made of overlapping bars. Previously, this theory has been applied to an integral beam. System identification results are presented for both simulated and experimental tests and they are compared with those predicted by means of finite element modeling. The lattice filtering approach works well for simulated data based on finite element modeling. However, considerable discrepancy exists between estimates obtained from experimental data and the finite element analysis. It is believed that this discrepancy is the result of inadequacies in the finite element modeling to represent the damped motion of the laboratory apparatus.

Introduction

The ability to predict the dynamic behavior of large space structures (LSS) adequately for control system design is doubtful because of their expected size, appreciable flexibility, and on-orbit assembly anomalies. Hence, dynamical modeling from on-orbit measurements, followed by modifying the control system as dictated by the identified control system design model (adaptive control), is of interest. The goal of this paper is to determine, using a generic grid structure, whether a priori modeling of the structure is adequate for a high authority control system design or whether on-orbit identification is needed.

An approach for identifying the dynamic behavior of LSS that estimates model order in addition to model parameters is presented in [1]. It uses lattice filters which provide an order as well as a time recursive algorithm for linear least squares signal estimation. [2] provides a tutorial on lattice filter theory and applications. The outputs of the theory of [1] are the least square estimate of the measurement sequence, the model order required to fit the measurements, the associated lattice model (this includes mode shape

[1]This paper was originally presented at the American Control Conference, San Diego, California, June 6-8, 1984.

[2]NASA Langley Research Center, Hampton, VA 23665.

[3]Old Dominion University Research Foundation, Hampton, VA 23666.

estimates that are orthonormal in the measurement space), and the associated auto-regressive moving average (ARMAX) model of the measurement sequence.

Some distributed adaptive control strategies require identification of the natural modes of a structure [3, 4]. Unfortunately, the lattice filter provides mode shapes that are orthonormal in the measurement space and, hence, are not the natural modes. Natural modes can be obtained, however, either through an eigenvector analysis of the identified ARMAX model or through a transformation that provides spectral decomposition of the lattice filter modal amplitudes [5]. The latter method is used herein to obtain the natural modes. Using spectral decoupling to determine mode shapes, one can obtain mode frequency and damping using an equation error parameter identification method [3] that employs a second-order ARMAX model to represent the natural mode amplitudes. The procedure of [3] tracks frequency and damping coefficients required for the modal amplitude input sequence to fit the second order ARMAX model. Because the input sequence may have an unfavorable signal to noise ratio, the parameters so derived must be tested for validity before use in control system design. This parameter testing is treated in detail in [6] but is not employed herein.

The foregoing procedure has been used to identify the dynamic characteristics of an integral free-free beam in [1, 7]. [8] describes the test apparatus used in those studies. In this paper, the theory is applied to a more complex, two-dimensional grid structure made of overlapping bars. First, a brief overview of the theory used is presented. Next, system identification results are presented using both simulated and experimental data. Finally, the experimental results are compared with those predicted using finite element modeling.

Summary of the Method Used to Identify Structural Dynamics Systems

For the application considered here we assume that the kth measurement sample is of the form

$$y_k^T = [y_1(k), y_2(k), \cdots y_{NS}(k)] \tag{1}$$

where NS represents the number of sensors. It is assumed that y is generated from a model system such that

$$y_k = \Phi\Psi_k + n_k \tag{2}$$

Here, Φ is a mode shape matrix, Ψ_k is the modal amplitude vector, and n_k is a Gaussian random variable with a zero mean and a covariance matrix R. Typically, for structural dynamics applications, each component of Ψ_k is the output of an uncoupled second-order process. The task here is to estimate the order and obtain the least square estimate of Ψ_k from $N + 1$ measurement samples y_0 through y_N. [1] presents a derivation of the equations that relate order n, and time i, recursions for the normalized forward and backward residuals (e and r, respectively) as well as the least squares estimate of the measurement vector y. These equations are listed below:

$$\mathbf{e}_{i,n+1} = (1 - k_{i,n+1}^2)^{-1/2}(\mathbf{e}_{i,n} - k_{i,n+1}\mathbf{r}_{i-1,n}) \tag{3}$$

$$\mathbf{r}_{i,n+1} = (1 - k_{i,n+1}^2)^{-1/2}(\mathbf{r}_{i-1,n} - k_{i,n+1}\mathbf{e}_{i,n}) \tag{4}$$

$$\hat{y}_N = \sum_{n=0}^{N-1} E(\mathbf{e}_{N,n} | \mathbf{r}_{N-1,n}) \tag{5}$$

with

$$k_{i,n+1} = \langle \mathbf{e}_{i,n}, \mathbf{r}_{i-1,n} \rangle \tag{6}$$

and $E(x|y)$ is the orthogonal projection operator of the vector x onto the vector y. The symmetry of the recursion formulae is apparent. The equations are coupled by the term $k_{i,n+1}$ which is customarily called the "reflection coefficient."

Clearly, in this approach one may "fit the noise" by continually increasing the order of the system; however, once the order of the estimator has increased sufficiently, the residual errors should lie within a noise band which can be predicted based on assumed noise characteristics. A threshold value can be selected based on this predicted noise band and order determined by a test of whether or not the residuals have been reduced to lie within the noise band. Also, the test can be made considering several samples of data; that is, using a data window. [1] documents experience in order determination based on this threshold test.

Having defined the order required to fit the data using a linear model, we seek a fixed set of basis functions that are spectrally decoupled for modal control. Therefore, a fixed orthonormal basis is used during intervals when the order estimate is constant. (However, the order estimate is checked at each measurement sample based on the threshold test.) The lattice filter uses the current measurement as the first mode shape and, using a modified Gram-Schmidt orthonormalization procedure, generates additional basis functions from estimation residuals. Consequently, the output of the lattice filter produces coupled mode shapes and corresponding modal amplitudes wherein the first coupled modal amplitude will contain all significant natural modes. Since the order estimate n has been determined, the first coupled mode digital Fourier transform (DFT) amplitude spectrum is searched for the n most significant peaks and corresponding frequencies. Because the spectrum contains n peaks for the n separate modes, a transformation matrix can be obtained that decouples the spectrum. This transformation matrix is the inverse of the matrix whose elements are the real part of the transform of the n coupled modal amplitude channels (rows) evaluated at the n peak frequencies (columns). It effectively transforms the lattice filter modes into spectrally decoupled natural modes. These decoupled modes are not orthogonal. This procedure is described in [5].

Thus, the decoupled modal amplitude time series, $w(k)$, is obtained by applying the transformation to the direct output of the lattice filter. This time series is then analyzed, for each mode, to identify the parameters of its autoregressive moving average ARMAX model. The inputs to each ARMAX modal model are the generalized forces and hence, each model takes on the form

$$w(k) = A_1 w(k-1) + A_2 w(k-2) + B_1 f(k-1) + B_2 f(k-2) \tag{7}$$

where f represents generalized forces. The parameters $p^T = (A_1, A_2, B_1, B_2)$ are the ones which are identified and which are required for the control law design process. Thus, the ARMAX model output error is

$$\begin{aligned} e(k-1) = w(k-1) - [&A_1(k-1)w(k-2) + A_2(k-1)w(k-2) \\ &+ B_1(k-1)f(k-2) + B_2(k-1)f(k-3)] \end{aligned} \tag{8}$$

The method of [3] is used to identify the parameters (p) using the iteration sequence

$$p(k) = p(k-1) + e(k-1) \cdot [W_1 w(k-2), W_2 w(k-3), W_3 f(k-2), W_4 f(k-3)] \quad (9)$$

As indicated in [3], the weights W_i ($i = 1, \ldots, 4$) must be selected so that they are consistent with the relation

$$W_1 w^2(k-2) + W_2 w^2(k-3) + W_3 f^2(k-2) + W_4 f^2(k-3) < 2 \quad (10)$$

and the inputs to the algorithm (w and f) must be sufficiently varying and large if the parameters are to converge to their correct value.

Damping ratios and natural frequencies of the modes can be obtained from A_1 and A_2 of equation (7). However, the solution is not unique, due to the foldover phenomenon of sampling. By finding the roots, z_i, of the characteristic equation (7) and using the relation $z_i = e^{h_i \tau}$ in the primary strip, where τ is the sampling period, the following equations for damping ratio and natural frequency are obtained for a typical root, say z:

$$\omega = \phi/(2\pi\tau) \quad (11)$$

$$\zeta = c(c^2 + \phi^2)^{1/2} \quad (12)$$

wherein

$$\phi = \tan^{-1}(b/a) \quad (13)$$

$$c = -\frac{1}{2}\ln(a^2 + b^2) \quad (14)$$

and $a = \mathrm{Re}(z)$ and $b = \mathrm{Im}(z)$. The behavior of this overall system identification methodology with both simulated and experimental data is discussed in the subsequent sections.

Description of the Flexible Grid Facility

Figure 1 shows the flexible grid experimental appartus currently being built at the NASA Langley Research Center. The grid is a 7 ft by 10 ft planar structure made by overlaying aluminum bars of rectangular cross section. The bars are centered every foot so that there are 8 vertical and 11 horizontal bars. As shown in Fig. 1, the grid is suspended by a cable at two locations on the top horizontal bar. The motions of the grid perpendicular to the plane of Fig. 2 are the ones of interest in this study. There are nine noncontacting deflection sensors mounted on a back frame which give a 9×1 measurement vector. The sensor data are linked to the main CYBER 175 Real-Time Computer System at NASA Langley Research Center so that the identification can be carried out in real time. For the experimental tests, the locations of the sensors are indicated in Fig. 2.

Simulation Studies

A finite element analysis of the grid was performed which included the suspension cables. Nodes were placed at each overlapping joint on the grid, the ceiling attachment points of the cable, and every one-half foot along the cable. The grid elements connecting the nodes were modeled as bending elements, whereas the cable elements were

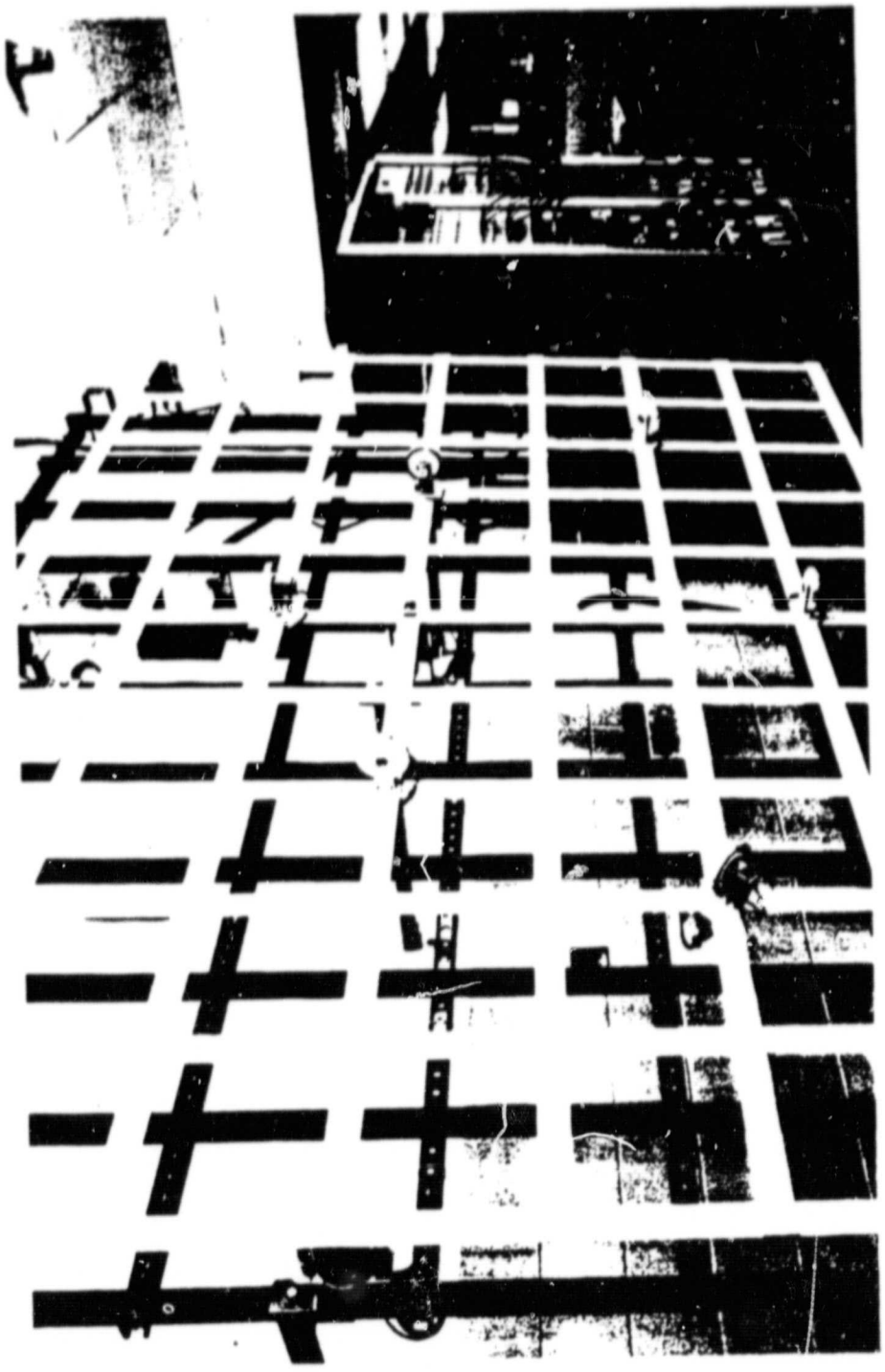

FIG. 1. A Photograph of the Grid Apparatus

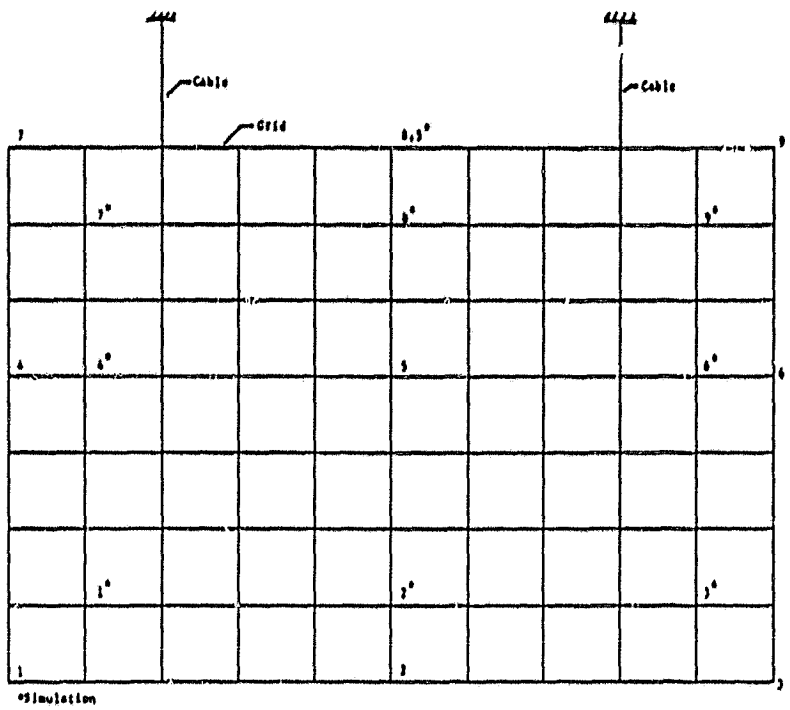

FIG. 2. A Schematic of the Grid Apparatus Indicating Locations Referred to in the Text and Subsequent Figures

modeled as two-force members. Thus, a total of 165 elements were included in the model. Four degrees of freedom appropriate for motion normal to the plane of the grid were considered. No damping was included in the model. Thirty modes were obtained from this analysis. The frequencies of the first ten modes are listed in Table 1. The first three modes are the pendulum modes, the fourth is the first bending mode and the fifth is the first torsional mode. The finite element analysis uses an iterative method to calculate mode frequencies. The frequencies used in simulation are believed to be numerically accurate since the change in eigenvalue iterate of the highest frequency mode used in the simulation is 10^{-11} on the final iteration. The corresponding eigenvalue iterate was 1565, which corresponds to the mode 8 frequency in Table 1.

A simulation was developed that accommodates the first 15 modes of the analysis, but only four modes were used herein. Modes 4, 6, 7, and 8 were used. A sampling rate of 32 Hz was simulated with a standard deviation for the measurement noise of 0.005 in. which was based on actual sensor characteristics. Modes were simulated with modal amplitude initial conditions of 0.1. The data window for order determination included eight samples. In this work, the sensor locations were chosen based on several simulations. These locations differ from those of the experimental apparatus in that they were selected to maximize the effect of simulated modes on the sensors. This was accomplished by visual examination of the simulated sensor outputs. The selected locations are indicated in Fig. 2. An asterisk is used to distinguish simulation sensor locations from experimental ones. One may expect that location 5 would be preferable

TABLE 1. Modal Frequencies Obtained from the Finite Element Analysis of the Grid

Mode Number	Frequency (Hz)
1	0.364
2	0.625
3	1.398
4	2.29
5	3.07
6	4.791
7	5.933
8	6.297
9	7.337
10	10.352

to location 5*; but, since some simulated modes had little input to a sensor at location 5, location 5* proved to be a better location.

Based on the entire measurement vector, the lattice filter order estimate is shown in Fig. 3. Also, sensor 5* data, typical of those of the other sensors, is shown in Fig. 3. After estimating the order, we carried out a transformation based on the discrete Fourier

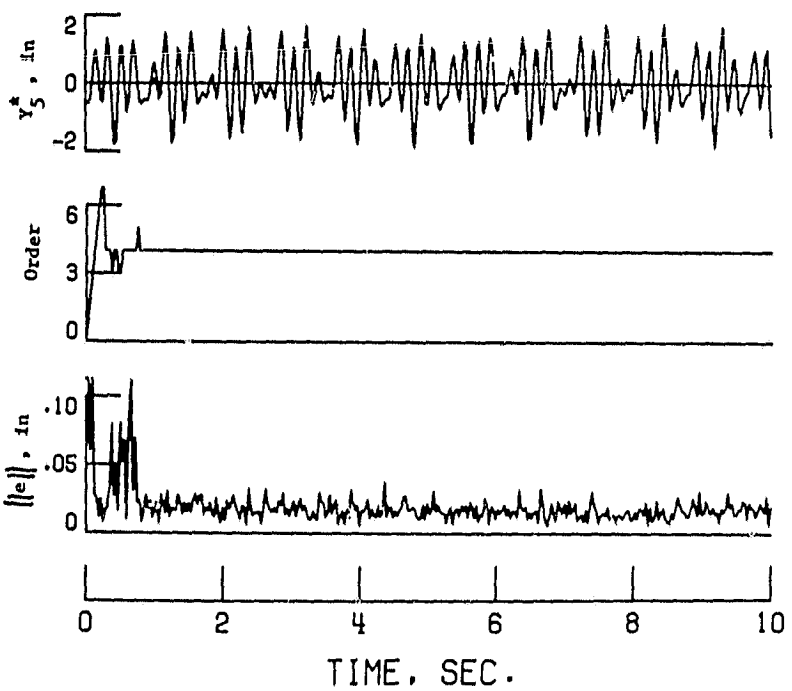

FIG. 3. Simulation Time Histories of Sensor 5*, Lattice Filter Order Estimate, and the Norm of the Estimation Error for the Entire Measurement Vector.

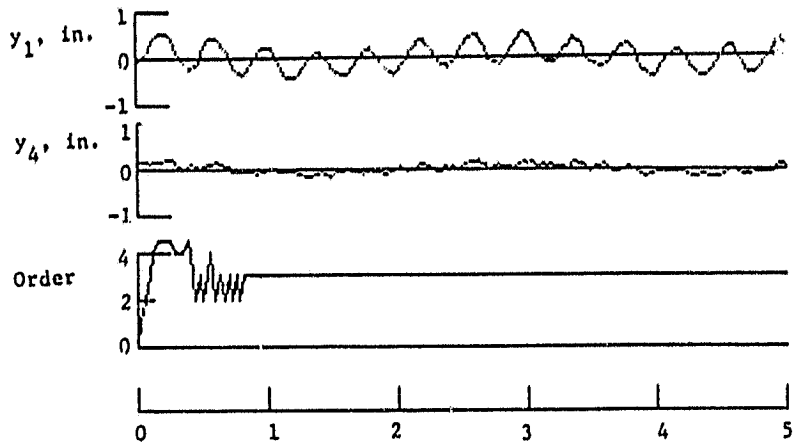

FIG. 4. Sensors 1 and 4 from Experimental Tape 5 and the Estimate of Signal Order Obtained by the Lattice Filter.

transform (DFT) using 128 samples in order to obtain the natural modes, and used the equation error method to identify associated modal frequencies and damping. The resulting modal frequencies, damping and mode shapes are compared with those predicted by finite element analysis in Table 2. The identification of frequencies and damping are close for all four simulated modes. However, the mode shape estimates agree with simulation for only three modes. One possible explanation for this is the limitation imposed by sampling rate and the number of samples used to decouple the lattice filter modes. Sampling at 32 Hz and including 128 data points in the DFT, a

TABLE 2. Comparison Between Simulated and Identified Results

	Mode 4		Mode 6		Mode 7		Mode 8	
	Simu-lated	Identi-fied	Simu-lated	Identi-fied	Simu-lated	Identi-fied	Simu-lated	Identi-fied
Frequency (Hz)	2.29	2.4	4.79	4.8	5.93	6.0	6.3	6.4
Sensor								
1*	0.29	0.30	−0.16	−0.17	0.31	0.32	0.59	0.45
2*	−0.40	−0.41	−0.12	−0.08	−0.43	−0.43	0	−0.43
3*	0.29	0.30	−0.16	−0.18	0.31	0.32	−0.16	0.21
4*	0.30	0.31	0.38	0.37	−0.06	−0.06	0.01	−0.09
5*	−0.39	−0.36	−0.72	−0.74	0.49	0.49	0.01	0.49
6*	0.30	0.30	0.37	0.36	−0.06	−0.06	−0.01	−0.06
7*	0.31	0.31	−0.20	−0.15	−0.32	−0.31	0.39	−0.19
8*	−0.39	−0.38	−0.26	−0.29	0.41	0.41	0	0.37
9*	0.31	0.31	−0.20	−0.14	−0.32	−0.31	−0.39	−0.38

frequency resolution of only 0.25 Hz is obtained. Since the expected frequency separation between modes 7 and 8 is only 0.4 Hz, good decoupling cannot be achieved.

To summarize the lessons learned from the simulation studies:

1. The least squares lattice filter gives good identification of simulated modal frequencies, damping ratios, and mode shapes in the presence of sensor noise expected in the experimental apparatus.
2. The DFT method of obtaining natural modes from the lattice modes is inaccurate if the modes are closely spaced in frequency. This may be improved by adding more samples to the DFT.
3. Sensor locations should be properly selected to insure good identification of simulated mode shapes.

The next section will discuss results obtained from the experimental apparatus.

Experimental Results

Experiments were conducted using the grid apparatus previously described. The grid was excited using an air shaker which periodically exhausted a jet of air that impinged on the grid at sensor location 1. The frequency of the jet was adjustable from 0 to 50 Hz. Although the resulting grid excitation was periodic, it was not purely sinusoidal but was rich in harmonics. Because of the range limits of the deflection sensors - 0 to approximately 2 in. - the maximum peak-to-peak deflections of the grid were limited to about 1 in. When the peak-to-peak deflection neared this limit, the air shaker was turned off and the grid was allowed to vibrate freely with only air and material damping. A CYBER 175 Real-Time Computer System sampled the deflection sensor data at 32 Hz for 5 seconds. The data were stored on a system data file for further analysis. Since only free-decay response data were recorded, the B_1 and B_2 parameters of equation (7) were not identifiable. Figure 4 presents data from file 5. Here, the order estimate is seen to converge to an oscillation between 2 and 3 at about 0.5 s. At about 0.8 s, the order estimate was fixed at 3 and data collection (at 32 Hz) for the 64 time samples required for the DFT was started. The DFT was accomplished at about 2.8 s and the decoupling transformation matrix was calculated. The modal amplitudes after this time should contain a single frequency and the transformed mode shapes should correspond to the excited natural modes of the structure. Thus, three modes were extracted from the experimental data tape. These have frequencies near 0.5 Hz, 2.5 Hz, and 5 Hz. Table 3 presents the mode shape estimates obtained from the experiment. Also presented are selected mode shape predictions taken from finite element analyses. The modes selected were those whose frequencies bracket the experimentally derived ones. The following discussion deals with the Table 3 data in order of increasing frequency.

A good comparison does not exist between the first or third experimental modes and either of their bracketing finite element analysis modes. Additionally, there is some bending in the first experimental mode as evidenced by sensors 4, 5, and 6. The amplitude of this mode is shown in figure 5 along with its ARMAX parameters A_1 and A_2 and their primary strip equivalents of damping and frequency. Figures 6 and 7 show the same information for the second and third modes, respectively. For the second mode, a good comparison does exist between it and the 3.07 Hz finite element analysis mode. Note that, however, the output of sensor 4 is opposite in sign and reduced in

TABLE 3. Comparison Between the Finite Element Predictions (P) and Experimental Identification (E)

	Mode 1 Comparisons			Mode 2 Comparisons			Mode 3 Comparisons		
Origin	P	E	P	P	E	P	P	E	P
Frequency (Hz)	0.364	0.5	0.625	2.29	2.3	3.07	4.79	5	5.93
Sensor									
1	−0.51	0.26	0.43	0.35	−0.45	−0.47	−0.36	−0.04	0.43
2	−0.51	0.46	0	−0.25	0.11	0	−0.34	−0.38	−0.35
3	−0.51	0.66	−0.45	0.35	0.44	0.48	−0.36	−0.14	0.43
4	−0.26	0.24	0.41	0.38	−0.08	0.13	0.22	0.18	−0.07
5	−0.26	−0.1	0	−0.25	0.05	0	0.24	0.10	0.07
6	−0.26	0.41	−0.41	0.38	−0.03	−0.13	0.22	−0.01	−0.07
7	−0.08	0.10	0.36	0.38	0.54	0.51	−0.38	−0.65	−0.45
8	−0.08	0.20	0	−0.24	−0.07	0	−0.43	0.29	0.32
9	−0.08	0.10	−0.36	0.38	−0.54	−0.51	−0.38	−0.54	−0.44

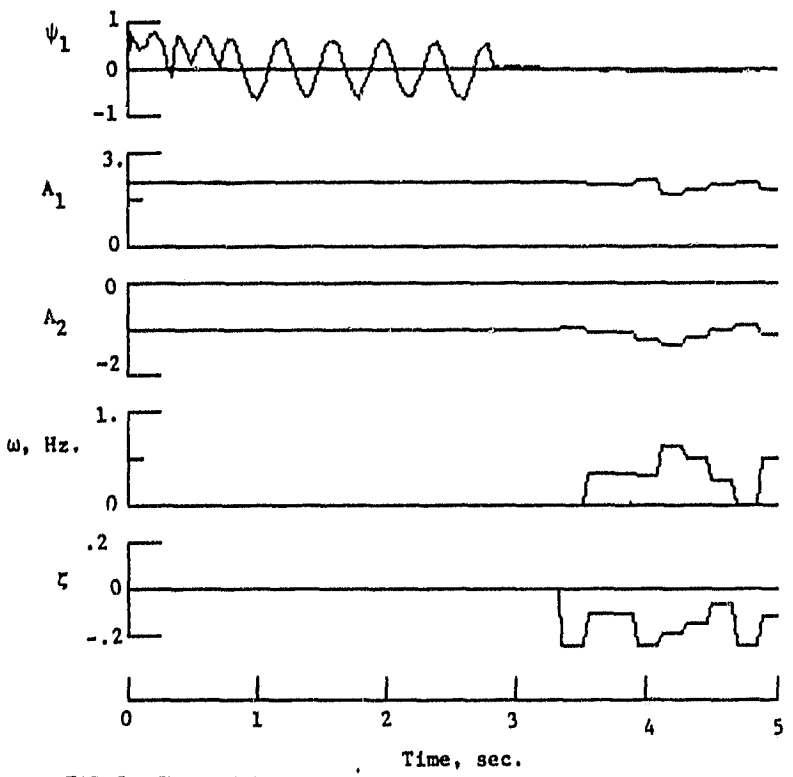

FIG. 5. Characteristics of the First Mode Identified from Experimental Tape 5.

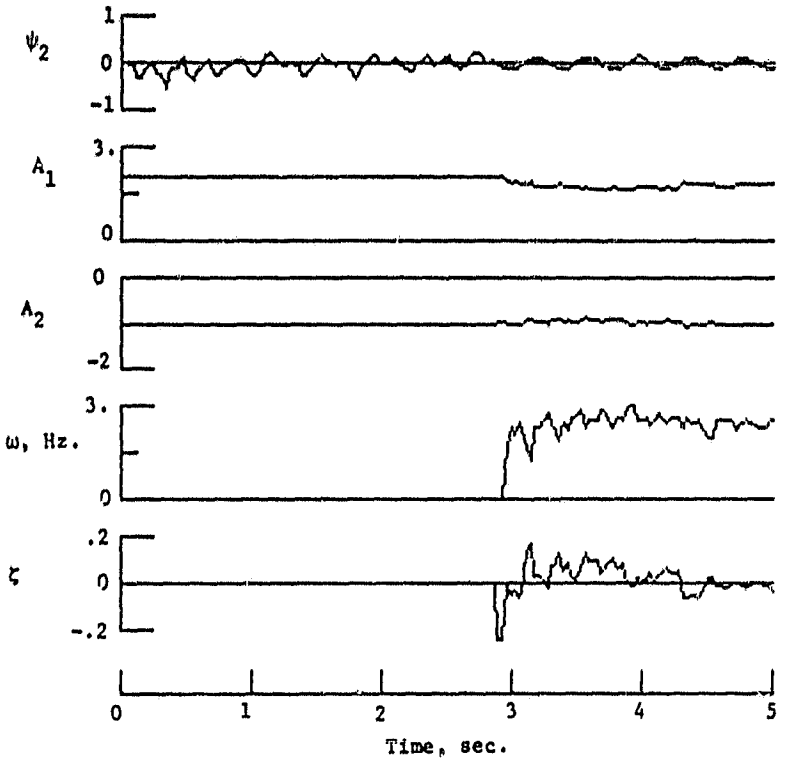

FIG. 6. Characteristics of the Second Mode Identified from Experimental Tape 5.

amplitude from the finite element prediction. This means that a feedback on that sensor based on the finite element analysis will be destabilizing near the 2.5 Hz frequency. The validity of this deduction can be established by examining the outputs of sensors 1 and 4 [4]. According to the finite element analysis, the 2.5 Hz content of the sensors should be opposite in sign. However, they are *in phase* in agreement with the identification results.

Conclusion

The application of the least squares lattice filter in system identification has been extended to a non-integral, two-dimensional grid structure made of overlapping bars. Previous experience has been limited to an integral free-free beam. Both simulation and experimental data were used to evaluate the system identification capabilities of the method. In the simulations, the least squares lattice filter gave good identification of simulated modal frequencies, damping, and mode shapes in the presence of sensor noise expected in the experimental apparatus. However, the spectral decoupling method of obtaining natural modes from lattice filter modes required a large number of data points in the discrete Fourier transform to get adequate frequency resolution when the modal frequencies were closely spaced. This problem can be overcome by an eigenvector analysis of the lattice filter's associated ARMAX model. When the lattice filter

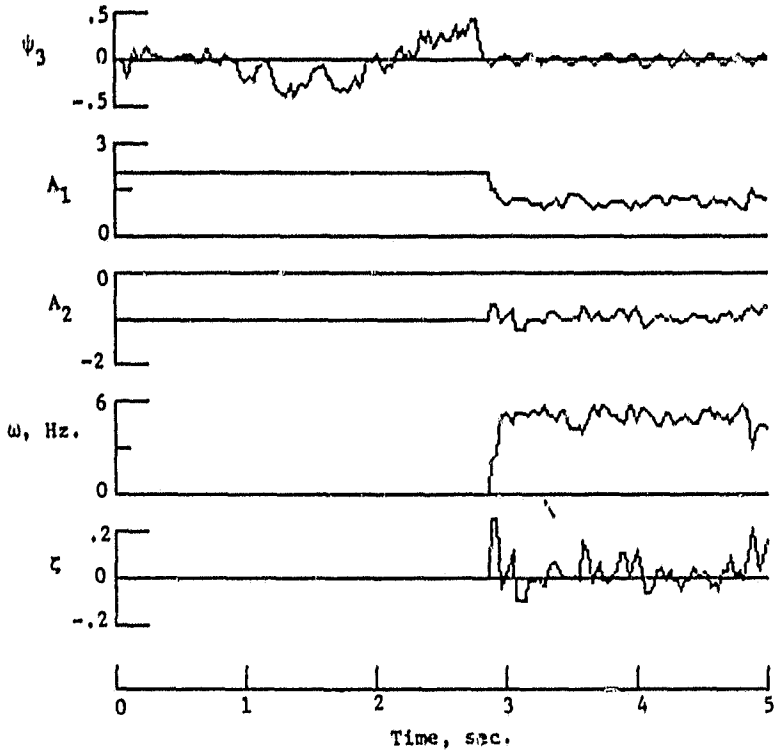

FIG. 7. Characteristics of the Third Mode Identified from Experimental Tape 5.

was used for system identification with experimental data, the mode shapes identified differed significantly from those of the finite element analysis. This has been corroborated by examination of the sensor data and indicates that on-line identification of large structural dynamic systems may be absolutely necessary to get acceptable performance in a high gain system that requires knowledge of mode shapes.

References

[1] SUNDARARAJAN, N. and MONTGOMERY, R. C. "Adaptive Identification for the Dynamics of Large Space Structures," *Proceedings of the 1982 AIAA Guidance and Control Conference*, Paper No. 82-1565, August 1982, pp. 379–387.

[2] FRIEDLANDER, B. "Lattice Filters For Adaptive Processing," *Proceedings of the IEEE*, Vol. 70, No. 8, August 1982, pp. 829–867.

[3] JOHNSON, C. R., JR. and MONTGOMERY, R. C. "A Distributed System Adaptive Control Strategy," *IEEE Transactions on Aerospace and Electronic Systems*, Vol. AES-15, No. 5, 1979, pp. 601–612.

[4] THAU, F. E., MONTGOMERY, R. C., and HORNER, G. C. "On-Line Structural Parameter Identification," *Proceedings of the AIAA Guidance and Control Conference*, Albuquerque, New Mexico, August 19-21, 1981, pp. 530–539.

[5] SUNDARARAJAN, N. and MONTGOMERY, R. C. "Decoupling the Structural Mode Estimated Using Recursive Lattice Filters," *Proceedings of the 21st IEEE Conference on Decision and Control*, December 1982, pp. 998–999.

[6] SUNDARARAJAN, N., WILLIAMS, J.P., and MONTGOMERY, R.C. "Parameter Testing for Lattice Filter Based Adaptive Modal Control Systems," *Proceedings of the AIAA Guidance and Control Conference*, August 1983, pp. 599–605.

[7] SUNDARARAJAN, N. and MONTGOMERY, R.C. "Experiments Using Lattice Filters for the Identification of Structural Dynamics," *Proceedings of the 24th AIAA/ASME/ASCE/AHS Structural Dynamics and Materials Conference*, Lake Tahoe, Nevada, Paper No. 83-0880-cp, May 2-4, 1983.

[8] MONTGOMERY, R.C., HORNER, G.C., and COLE, S.R. "Experimental Research on Structural Dynamics and Control," *Proceedings of the Third VPI & SU/AIAA Symposium on Dynamics and Control of Large Flexible Spacecraft*, June 1981, pp. 365–377.

APPENDIX B

EXPERIMENTAL EVALUATION OF FLEXIBLE STRUCTURE IDENTIFICATION USING LATTICE FILTERS

EXPERIMENTAL EVALUATION OF FLEXIBLE STRUCTURE IDENTIFICATION USING LATTICE FILTERS

By

N. Sundararajan
Old Dominion University Research Foundation
NASA Langley Research Center
Hampton, VA USA

To be presented at the
7th IFAC Symposium on Identification
and System Parameter Estimation
York, England
July 2-8, 1985

EXPERIMENTAL EVALUATION OF FLEXIBLE STRUCTURE IDENTIFICATION USING LATTICE FILTERS

N. Sundararajan

Old Dominion University Research Foundation, NASA Langley Research Center, Hampton, VA

Abstract. This paper presents the use of least square lattice filters in identification of the dynamics of highly flexible structures. Lattice filters have been used extensively in the areas of adaptive signal procesing and speech synthesis. Herein, they are used for on-line identification of the number of modes, mode shapes and modal amplitude time series from the measurement data. The theory is illustrated using experimental data for a simple free-free beam and a more complex, flexible, two-dimensional grid apparatus. Results presented indicate that the lattice filter approach produces effective identification of structural dynamics for the class of structures studied to this time.

Keywords: Identification, Lattice Filters, Space Vehicles, Least Squares Approximation, Vibration Measurements.

INTRODUCTION

With the size of the structures currently contemplated for building in space becoming larger, identification of the dynamic characteristics of these structures is an important area of research. Accurate on-orbit identification becomes a necessity as these structures cannot be assembled fully on the ground because of its size, and also it is difficult to predict an accurate model on the ground. As the performance requirements for these structures in space become stringent, however, it becomes imperative to identify their charecteristics on-orbit and modify the control system as dictated by the identified control system design model (adaptive control). This paper highlights the model determination phase of the adaptive control problem. This phase involves not only determination of parameter estimates for an assumed linear form, but also the order of the linear model form.

An approach for identifying the dynamics of Large Space Structures (LSS) that estimates model order in addition to model parameters is presented in Sundararajan and Montgomery (1983). It uses lattice filters which provide an order as well as time recursive algorithm for linear least square signal estimation. A comprehensive tutorial on the theory and applications of lattice filters has been given by Freidlander (1980). The main results from the paper of Sundararajan and Montgomery (1983) are: the least square estimate of the measurement sequence; the model order required to fit the measurements; the associated lattice model (this includes mode shape estimates that are orthonormal in the measurement space) and the associated auto-regressive moving average (ARMA) model of the measurement sequence. The mode shapes obtained by the lattice filter are not the "natural" modes but a linear combination of them. In order to compare the identified mode shapes to those predicted by finite element analysis, a decoupling method to obtain natural mode shapes from the lattice mode shapes have been developed in Sundararajan and Montgomery (1982). Using the above spectral decoupling method to obtain natural mode shapes, mode frequency and damping can be obtained using an equation error parameter identification method (Johnson and Montgomery (1979)) that employs a second order ARMA model to represent the natural mode amplitudes. This procedure is followed herein.

The objective of this paper is to present the experience in using lattice filter theory for identification of structural dynamics of two flexible structures. They consist of a one-dimensional free-free beam and a two-dimensional flexible grid apparatus. The structures are part of an experimental facility at the Aerospace Control Laboratory at NASA Langley Research Center for studying advanced control concepts for large space structures. The beam apparatus provides a simple structure to test the basic concepts first, and the grid apparatus provides a more complex structure close to the real spacecraft. Before presenting the results of lattice filter identification for these structures, a brief outline of the basic theory is given. Results are presented for the identification of the dynamics of the beam using experimental data. Next, the same is repeated for the grid apparatus. Conclusions based on the above study results are then summarized.

Summary of Lattice Filter Identification Theory

For the application considered here, we assume that the kth measurement sample is of the form

$$y_k = \left[y_1(k),\ y_2(k),\ \ldots,\ y_{NS}(k) \right]$$

where NS represents the number of sensors. It is assumed that y is generated from a model system wherein

$$y_k = \phi q_k + n_k \qquad (1)$$

Here, ϕ is an NSxNM mode shape matrix, q_k is the NMx1 modal amplitude vector, and n_k is a NSx1 gaussian random variable with zero mean and a covariance matrix R. Typically, for structural dynamics applications, each component of q_k is the output of an uncoupled second order process. The task here is to estimate the order (NM) and

obtain the least square estimate of q_k from the N+1 measurement samples y_0 through y_N.

Sundararajan and Montgomery (1983) present a derivation of the equations that relate order, n, and time, i, recursions for the normalized forward and backward residuals as well as the least square estimate of the measurement vector. These equations are listed below:

$$\underline{e}_{i,n+1} = (1 - k^2_{i,n+1})^{-1/2}(\underline{e}_{i,n} - k_{i,n+1}\underline{r}_{i-1,n})$$

$$\underline{r}_{i,n+1} = (1 - k^2_{i,n+1})^{-1/2}(\underline{r}_{i-1,n} - k_{i,n+1}\underline{e}_{i,n})$$

$$\hat{y}_N = \sum_{n=0}^{N-1} \mathcal{E}(\underline{e}_{N,n} \,|\, \underline{r}_{N-1},n) \qquad (2)$$

wherein

$$k_{i,n+1} = \langle \underline{e}_{i,n}, \underline{r}_{i-1,n} \rangle$$

and $\mathcal{E}(x|y)$ is the othogonal projection operator of the vector x onto the vector y. The symmetry of the recursion formulae are apparent. The equations are coupled by the term $k_{i,n+1}$ which is customarily called the "reflection coefficient." The structure of this equation is depicted in Fig. 1 where we have used the symbol z^{-1} to represent the time shift operator, i.e.

$$z^{-1}r_{i,n} = r_{i-1,n}$$

It should be noted at this point that the lattice filter is a modified Gram-Schmidt procedure involving both forward and backward residuals wherein the backward residuals form an orthogonal basis for the entire observation sequence. Hence, any least square estimate is the orthogonal projection onto this basis. Assuming at this point the order NM has been obtained (which is explained below), the lattice filter has decomposed the estimation of y into the form of equation (1),

wherein

$$\phi = [r_{i,1}, \ldots r_{i,NM}]$$

and

$$\underline{e}_{i,NM} = q(i)$$

i.e., the backward residuals $r_{i,n}$ form the orthonormal basis, or the mode shape matrix ϕ and the forward residual $\underline{e}_{i,n}$ represents the modal amplitude time series.

The lattice filter has the following advantages:

1. Given a basis for order N, a basis for order N+1 can be obtained using the recursion formulae.

2. Because of the modified Gram-Schmidt procedure, the basis for all orders n between 0 and N are the first n elements of the basis of order N.

3. The estimate assuming any order n between 0 and N+1 can be computed using equation (2).

This lattice filter provides the information needed to determine the residual sequence for any model order between 0 and N+1 inclusive. This information provides the basis for the model order determination method described next.

Clearly, in this approach one may "fit the noise" by continually increasing the order of the system; however, once the order of the estimator has increased beyond the correct order, then the residual errors should lie within a noise band which can be predicted based on assumed noise characteristics. A threshold value can be selected based on this predicted noise band, and order can be determined by a test of whether or not the residuals have been reduced to lie within the noise band. Also, the test can be made considering several data samples when using a data window. Sundararajan and Montgomery (1983) document the experience in choosing the data window size NW and the threshold level based on simulations. Having defined the order required to fit the data using a linear model, for comparison with finite element analysis predictions, we seek a fixed set of basis functions that are spectrally decoupled. A method to obtain the decoupled modes from the lattice filter modes using digital Fourier transform (DFT) has been presented in Sundararajan and Montgomery (1982). Essentially, at this point we have estimates for order NM, mode shapes ϕ and modal amplitude time series q(k) from the lattice filter.

Since the ultimate objective of identification is for control system design, an ARMA model is identified using the modal amplitude time series q(k). The method is based on an equation error method described in Johnson and Montgomery (1979). For each mode, the model is described by the equation:

$$q(k-1) = A_1 q(k-2) + A_2 q(k-3) + B_1 u(k-2) + B_2 u(k-3) \qquad (3)$$

The equation error is given by:

$$e(k-1) = q(k-1) - \hat{q}(k-1)$$

$$= q(k-1) - \{\hat{A}_1 q(k-2) + \hat{A}_2 q(k-3)$$

$$+ \hat{B}_1 u(k-1) + \hat{B}_2 u(k-3)\}$$

where $\hat{q}$ is the model amplitude estimated by the lattice filter, u is the modal control force, k is the sample number and A_1, A_2, B_1, B_2 are the ARMA coefficients. The term in brackets is the model equation. The ARMA coefficients are then updated by:

$$\begin{bmatrix} \hat{A}_1(k) \\ \hat{A}_2(k) \\ \hat{B}_1(k) \\ \hat{B}_2(k) \end{bmatrix} = \begin{bmatrix} \hat{A}_1(k-1) \\ \hat{A}_2(k-1) \\ \hat{B}_1(k-1) \\ \hat{B}_2(k-1) \end{bmatrix} + e(k-1)\mu \begin{bmatrix} q(k-2) \\ q(k-3) \\ q(k-2) \\ q(k-3) \end{bmatrix}$$

The weight μ assures stability if

$$0 < \mu < 2/\{q^2(k-2) + q^2(k-3) + u^2(k-2) + u^2(k-3)\}$$

This identifier performs well in a low noise environment, but when the information content of the signal is small, it attempts to fit the noise (Thau, et. al. (1982). Also, the ideal ARMA model for the beam has input parameters (B's) which are three orders of magnitude smaller than the (A's). This causes a very high sensitivity to noise in the identification of the B's, and when the input force is applied, it tends to cause the identifier gain on the A's to decrease significantly.

Although these effects are evident in the results presented here, they did not prevent successful identification.

If one is interested in determining the damping ratios and natural frequencies of the modes, they can be obtained in a straightforward manner from the equation (3). However, it should be noted that this is not unique due to the foldover phenomenon due to sampling. by finding the roots of the equation (3) and using the relation $z = e^{sT}$ in the primary strip, where T is the sampling period, the damping ratio and natural frequency can be obtained.

The behavior of this overall system identification methodology with experimental data is discussed in the subsequent sections.

Experimental Studies for the Identification of a Free-free Beam

In this section, the lattice filter theory developed earlier is illustrated for the identification of a one-dimensional free-free beam. The identification scheme yields the structural dynamic characteristics of the beam. The experimental apparatus for the free-free beam is shown in Fig. 2. It consists of a 12-foot beam of rectangular cross-section which is suspended from the ceiling by two cables and is attached to four electromagnetic force actuators. There are nine noncontacting deflection sensors that measure the translational deflection of the beam. The actuators are compensated to eliminate the effects of friction as much as possible. This compensation is nonlinear, producing a force in the direction of the beam motion at the actuator attachment points which is designed to equalize the effect of friction. Testing was done by manually exciting the beam approximately in its first flexible mode and sampling the nine sensors at 64 samples per second. A total of 5 seconds of data was stored on a tape which was post processed with the algorithm. Figure 3 shows a time history of some of the measurement data processed by the algorithm. The innovations sequence for sensor 4, $INOV_4$, is shown just below its time history.

Also shown is the norm of the forward estimation residual, ENORM, which includes all components of the measurement vector. Below the norm is the estimate of model order. This was obtained using a data window of eight samples. Initially, the order estimator fills the data window, and hence, the indicated order estimate increases to 8. After this the order estimator settles to 2 indicating that, even though we attempted to excite only one mode, there were, in fact, two significant modes excited. Note also that the norm of the forward estimation error is small compared with the value at the start of the process when the order estimate was settling.

The modal amplitudes obtained from the lattice filter are spectrally decoupled, using the procedure discussed earlier, after enough data are taken to accurately take the DFT (64 time samples, about 1 second). This occurs at about 1.75 seconds, the first .75 seconds being used for the identification of mode shapes and model order (see Fig. 4). Figure 4 shows the modal amplitudes for both of the identified modes. These are the signals that are inputs to the parameter identification scheme used to identify the parameters of the ARMA model of the modes. The identified ARMA parameters are shown on Fig. 4 for each of the two modes identified. The a priori parameter estimates are initially offset from the values predicted by a finite element analysis which are also indicated in Fig. 4. These parameters track the instantaneous value required to minimize the output error. One possible explanation of the oscillatory behavior of the mode 2 parameter estimates is the nonlinearity of the actuator compensation. Nonlinearity is apparent in the sensor 6 data on Fig. 3. Note that lattice filter produces a linear least square fit of the data to the measurements, and in so doing, produces a predominantly linear first mode estimate and lumps the nonlinear dynamics into the higher modes. Thus, the parameter tracking is more stable in mode 1 and produces estimates of an undamped (A2=-1) oscillation at nearly 2.7 Hz. If the algorithm is constrained to an order estimate of one, the predominant response is linear, however, the fit error is increased by an order of magnitude.

The mode shapes estimates obtained from the lattice filter are shown in Fig. 5. In this figure we compare the estimates obtained by three methods, one analytic, and two experimental. The analytic result is the primary mode shape of the beam using Euler-Bernoulli theory. The two experimental results which are in substantial agreement are the nonlinear least squares algorithm of Thau, et al. (1982) and the lattice filter algorithm of this paper. Again note that there is apparently an effect of the four attached actuators on the dynamics of the test article. The lattice filter produces two modes, one near the mode of Thau et al. (1982) and another that is shown on Fig. 5. This other estimated mode does not resemble any mode analytically predicted using linear Euler-Bernoulli theory, rather, is required to model the effect of nonlinearities in the apparatus.

Experimental Studies for the Identification of a Flexible Grid

Next, the lattice filter identification scheme is tested in a more complex structure compared to that of the beam. The candidate structure considered is that of a two-dimensional flexible grid. Identification results are given using the experimental data obtained from the laboratory apparatus.

Figure 6 shows the flexible grid experimental apparatus in the Aerospace Control Laboratory, at NASA Langley Research Center. The grid is a 7 ft x 10 ft planar structure made by overlaying aluminum bars of rectangular cross section. The bars are centered every foot so that there are 7 vertical and 11 horizontal bars. As shown in Fig. 6, the grid is suspended by a cable at two locations on the top horizontal bar. The motions of the grid perpendicular to the plane of Fig. 6 are the ones of interest in this study. There are nine noncontacting deflection sensors mounted on a back frame which give a 9x1 measurement vector. The sensor data is linked to the main Cyber 175 Real Time Computer System at NASA Langley Research Center so that the identification can be carried out in real time.

In order to compare the experimental results of lattice filter identification of the flexible grid facility with predicted values, a finite element anlaysis of the grid was made which included the suspension cables. Four degrees of freedom appropriate for motion normal to the plane of the grid were considered. No damping was included in the model.

Experiments were conducted using the grid apparatus described above. The procedure for conducting the experiments was to excite the grid using an air shaker. The shaker was capable of periodically exhausting a jet of air that impinged

on the grid at sensor location 1 which was at the bottom left hand corner of the grid. The frequency of the jet was adjustable from 0 to 50 Hz. The resulting grid excitation was not purely sinusoidal but was rich in harmonics. Because of the range limits of the deflection sensors - 0 to approximately 2 in. - the maximum peak to peak deflections of the grid were limited to about 1 in. When the peak to peak deflection neared this limit, the air shaker was turned off and the grid was allowed to vibrate freely with only air and material damping. A Cyber 175 real time computer system sampled the deflection sensor data at 32 -Hz. for 5 sec. The data was stored on a system data file for further analysis. This test procedure was repeated for several shaker frequencies in the range of 1 to 10 Hz. This range has an upper limit because of the sampling frequency (32 Hz.) The lower limit is selected to include the predicted lowest vibration mode (2.2 Hz.) Eight data sets corresponding to different shaker excitation frequencies were created and stored on tapes. The following discussion pertains to results extracted from data set five.

Figure 7 presents data from sensors 1 and 4 as well as the lattice filter order estimate. For this case the order estimate was based on a data window of 8 samples and spectral decoupling was done with 64 time samples. From the figure, the order estimate is seen to converge to an oscillation between 2 and 3 at about .5 sec. At about .8 sec, the order estimate was fixed at 3 and data collection of the 64 time samples required for the DFT was started at 32 Hz. The DFT was accomplished at about 2.8 sec and then the decoupling transformation matrix was calculated. The modal amplitudes after this time should contain a single frequency and the transformed mode shapes should correspond to the natural modes of the structure which were excited. In that manner, three modes were extracted from experimental data tape 5. These have frequencies near .5Hz, 2.5 Hz., and 5 Hz. Table 1 presents the mode shape estimates obtained from the experiment. Also presented are selected mode shape predictions taken from finite element analyses. The modes selected were those whose frequencies bracket the experimentally derived ones. The following discussion deals with the Table 1 data in order of increasing frequency. A good comparison does not exist with either bracketing finite element analysis mode and the first experimental mode. Additionally, there is some bending in the experimental mode as is evidenced by sensors 4, 5, and 6. The modal amplitude for this mode is shown in Fig. 8 along with the ARMA parameters A_1 and A_2 for the mode and their primary strip counerparts of damping ζ and frequency ω. For the second mode, a good comparison does exist betwen it and the 3.07 Hz finite element analysis mode. Note that, however, the output of the sensor 4 is opposite in sign and reduced in amplitude from the finite element prediction. This means that a feedback on that sensor based on the finite element analysis will be destabilizing near the 2.5 Hz frequency. The validity of this deduction can be established by examining the outputs of sensors 1 and 4 (Fig. 7). According to the finite element analysis, the 2.5 Hz content of the sensors should be opposite in sign. However, they are in phase in agreement with the identification results.

CONCLUSION

The application of least square lattice filters in identifying the dynamic characteristics of highly flexible structures has been presented. The theory has been used to identify the structural characteristics of two experimental hardware, namely that of a free-free beam and a flexible grid structure. The results indicate that the lattice filter can be effectively used for on-line identification of the number of modes, mode shapes, modal damping and modal frequencies from the measurement data. The experimental results also indicate that there is considerable disagreement between them and analytical predictions. Based on these experimental studies, the main conclusion that can be drawn is that for large space structures, on-orbit testing and identification is essential before control is attempted.

REFERENCES

Friedlander, B. (1980). Lattice Filters For Adaptive Processing. Proceedings of the IEEE, 70, pp. 827-867.

Johnson, C. R., Jr. and R. C. Montgomery (1979). A Distributed System Adaptive Control Strategy. IEEE Transactions on Aerospace and Electronic Systems, AES-15, pp. 601-612.

Sundararajan, N., and Montgomery, R. C. (1982). Decoupling The Structural Mode Estimated Using Recursive Lattice Filters, Proceedings of the 21st IEEE Conference on Decision and Control, pp.998-999.

Sundararajan, N., and Montgomery, R. C. (1983). Identification of Structural Dynamics System Using Least Square Lattice Filters. Journal of Guidance, Control and Dynamics, 6, pp. 374-381.

Thau, F. E., Eliazov, T., E., and Montgomery, R. C. (1982). Least Square Sequential and Parameter and State Estimation for Large Space Structures. Proceedings of the 1982 American Control Conference, pp. 16-21.

Table 1.- Comparison Between the Finite Element Predictions and Experimental Identification

	Mode 1 Comparisons			Mode 2 Comparisons			Mode 3 Comparisons		
Origin	P	E	P	P	E	P	P	E	P
Freq. Hz	.364	.5	.625	2.29	2.5	3.07	4.79	5	5.93
Sensor									
1	-.51	.26	.45	.35	-.45	-.47	-.36	-.04	.43
2	-.51	.46	0	-.25	.11	-.00	-.34	-.38	-.35
3	-.51	.66	-.45	.35	.44	.48	-.36	-.14	.43
4	-.26	.24	.41	.38	-.08	.13	.22	.18	-.07
5	-.26	-.1	0	-.25	.05	0	.24	.10	.07
6	-.26	.41	-.41	.38	-.03	-.13	.22	-.01	-.07
7	-.08	.10	.36	.38	.54	.51	-.38	-.65	-.45
8	-.08	.20	0	-.24	-.07	0	-.43	.29	.32
9	-.08	.10	-.36	.38	-.54	-.51	-.38	-.54	-.44

P - Prediction based on finite element analysis
E - Calculation based on identification from experimental data

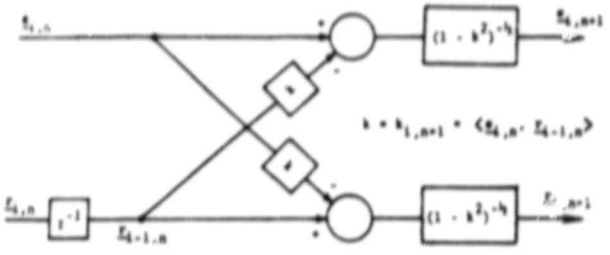

Fig. 1 Flow diagram of lattice section

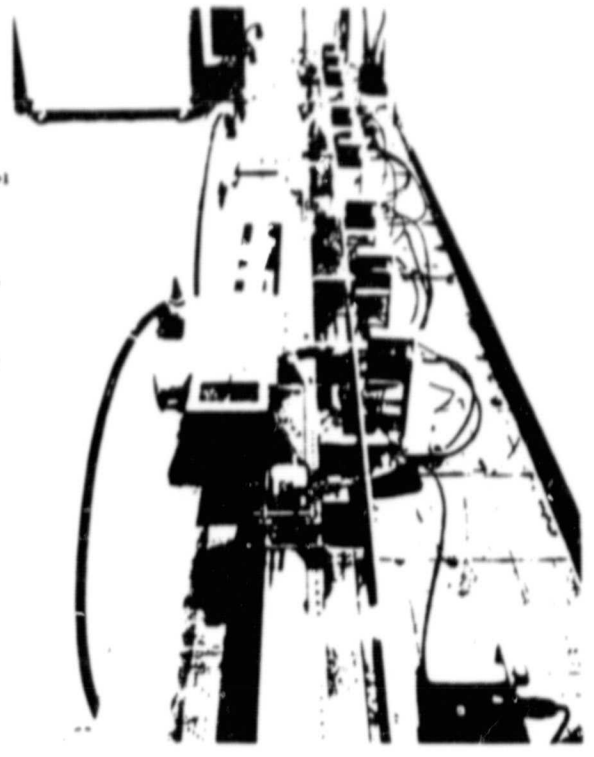

Fig. 2 A photograph of the beam apparatus

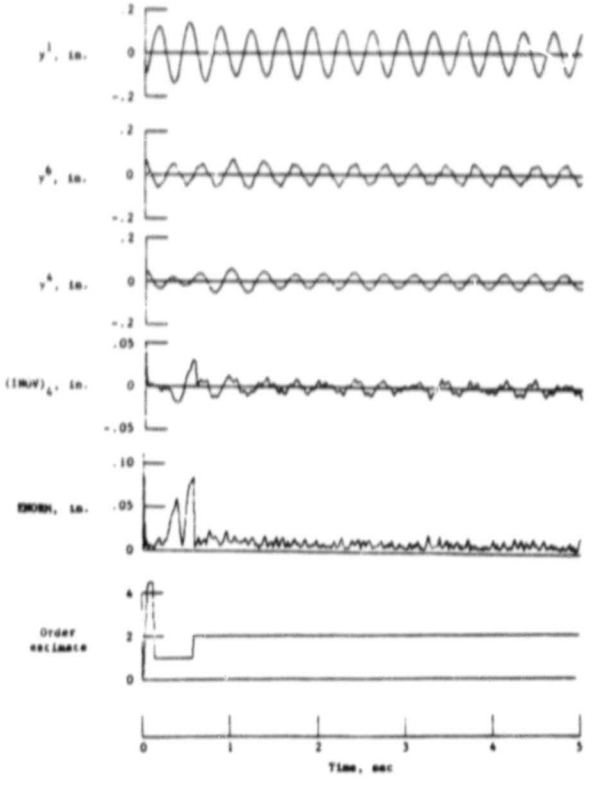

Fig. 3 Data relevant to the real time processing of the algorithm

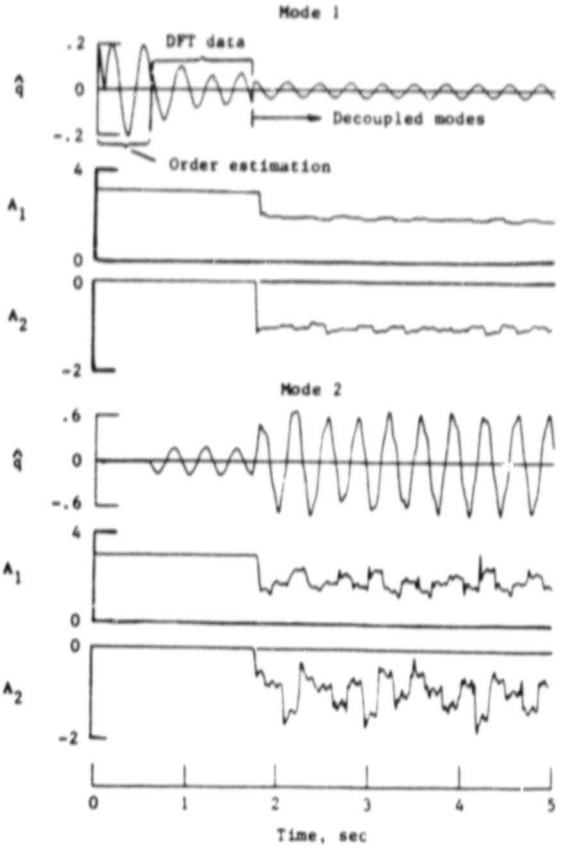

Fig. 4 Estimated modal amplitudes and identified ARMA parameters resulting from the algorithm

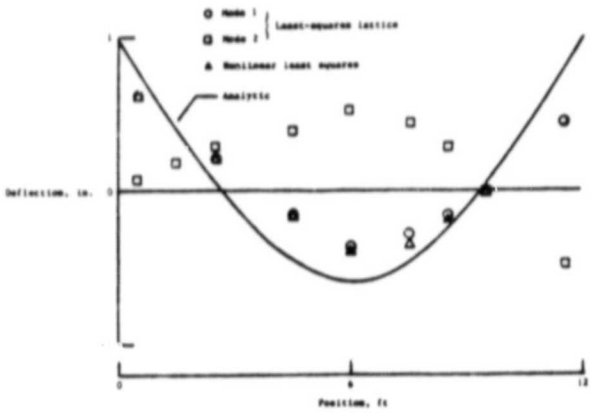

Fig. 5 Mode shape estimates obtained from the algorithms and a comparison with an analytic prediction and the estimates obtained using the nonlinear least squares technique of Thau.

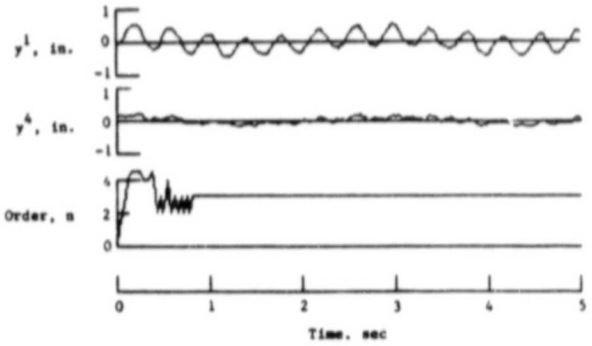

Fig. 7 Sensor 1 and 4 from experimental tape 5 and the estimate of signal order obtained by the lattice filter

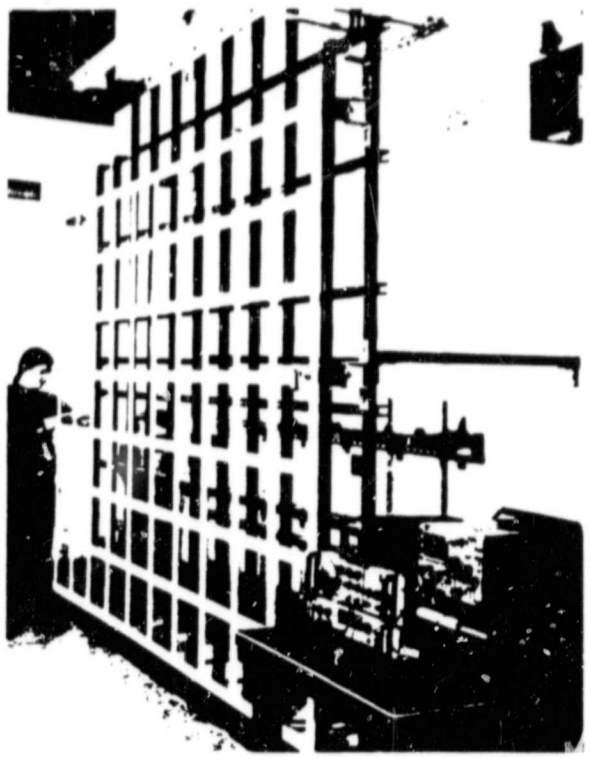

Fig. 6 A photograph of the flexible grid apparatus.

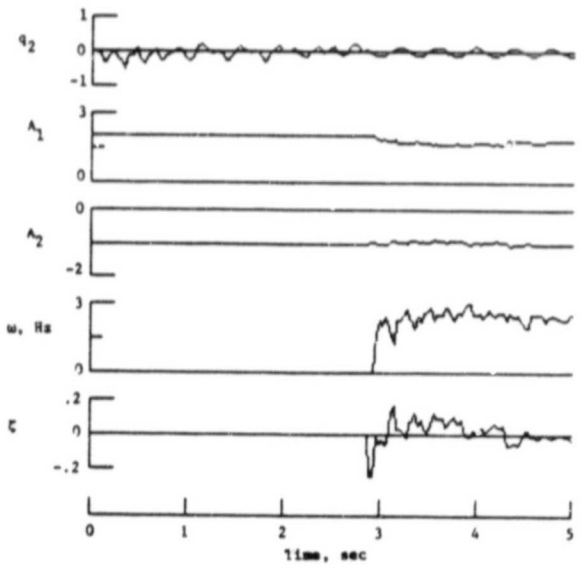

Fig. 8 Characteristics of the second mode identified from the experimental tape 5.

APPENDIX C

PROGRESS IN ADAPATIVE CONTROL OF FLEXIBLE SPACECRAFT USING LATTICE FILTERS

PROGRESS IN ADAPTIVE CONTROL OF FLEXIBLE SPACECRAFT USING LATTICE FILTERS

by

N. Sundararajan
Old Dominion University Research Foundation
Hampton, VA

and

Raymond C. Montgomery
NASA Langley Research Center
Hampton, VA

Workshop on Applications of Adaptive Control
Yale University, New Haven, CT
May 29-31, 1985

PROGRESS IN ADAPTIVE CONTROL OF FLEXIBLE SPACECRAFT USING LATTICE FILTERS

N. Sundararajan
Old Dominion University Research Foundation

Raymond C. Montgomery
NASA Langley Research Center

ABSTRACT

This paper reviews the use of the least square lattice filter in adaptive control systems. Lattice filters have been used primarily in speech and signal processing, but they have utility in adaptive control because of their order-recursive nature. They are especially useful in dealing with structural dynamics systems wherein the order of a controller required to damp a vibration is variable depending on the number of modes significantly excited. Applications are presented for adaptive control of a flexible beam. Also, difficulties in the practical implementation of the lattice filter in adaptive control are discussed.

INTRODUCTION

For large flexible spacecraft, design models will probably not be adequate. Hence, an adaptive control system is highly desirable. Early research into adaptive vibration control of large flexible structures is reported in reference 1. Therein, adaptive control of a spinning annular momentum control device (AMCD) was studied. That scheme consisted of simultaneous identification and control with the objective of regulating the out-of-plane deflections of the spinning AMCD. Some of the disadvantages of the method were the requirement of selecting the number of modes to be used for controller design, the use of analytically predicted mode shapes, and the coupling between modes due to inhomogenities in the system. Lattice filter adaptive control is a new method which attempts to overcome these problems. It is, hence, well suited for the adaptive control of flexible spacecraft.

The least square lattice filter has been used extensively in the field of speech and signal processing (reference 2). In these applications the filter is designed based on a predetermined estimate of system order. Reference 3 is a comprehensive tutorial on this subject. Concerning adaptive control, reference 4 proposes a self-tuning controller configuration using lattice filters. This scheme requires computing the polynomial coefficients for the plant and controller at each iteration and enforcing a known feedback structure for the controller. Reference 5 proposes inverting the transfer function of the plant for general adaptive control. This idea, with the least mean squares (LMS) algorithm, was utilized in reference 6 to obtain adaptive control. Reference 7 proposes a similar approach using lattice forms instead of the LMS algorithm. Reference 8 takes this approach but uses a lattice model instead of an autogressive, moving average with exogenous variables (ARMAX) model where familiar controller techniques could be used. All of these scheaes attempt simultaneous identification and control or direct adaptive control. For each case stability questions are not resolved analytically; neither are simulation results available in the open literature.

As opposed to simultaneous identification and control, the scheme discussed herein consists of conducting tests to obtain a design model, validating the model, designing a controller based on the validated model, and finally, engaging the control system. This approach is ideally suited to the control of large flexible spacecraft because of the passive environment of outer space and the potential of relaxation to a controller that is known to be stable - that of collocated rate feedback. It was originally presented in reference 9 and represented the first use of a recursive variable order structure for adaptive control. Therein, the lattice filter was used to provide an on-line estimate of the system order, mode shapes, and modal amplitudes to provide a validated modal control design model. After the identified model parameters are validated through a series of test procedures, they are used in a modal pole-placement control law design. Figure 1 shows the adaptive control scheme using lattice filters.

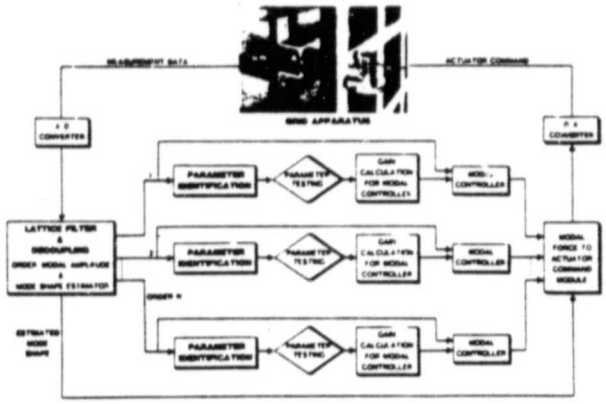

Figure 1.- Adaptive Control with Lattice Filters.

The purpose of this paper is to assess progress in using lattice filters in adaptive control of flexible spacecraft and to highlight problem areas for further research. First, lattice filter theory and order determination is summarized following the original development of reference 10. Then, their use in adaptive control is discussed along with applications to the vibration control of a beam. Finally, difficulties arising in the practical implementation are discussed.

SUMMARY OF LATTICE FILTER THEORY AND ORDER DETERMINATION

For application considered herein, we assume that the ith measurement sample is of the form

$$y_i^T = [y_1(i),\ y_2(i),\ \ldots,\ y_{NS}(i)]$$

here NS represents the number of sensors. It is assumed that y is generated from a model system wherein

$$y_i = \Phi \cdot \Psi_i + v_i \qquad (1)$$

Here, Φ is an NS x NM mode shape matrix, ψ_i is the NM x 1 modal amplitude vector, v_i is a Gaussian-random variable with zero mean and covariance matrix R. NM represents the number of modes in the system or order of the system.

Reference 10 presents a derivation of the equations that relate any order, n, and time, i, recursions for the normalized forward and backward residuals as well as the least square estimate of the measurement vector. These equations are listed below:

$$\underline{e}_{i,n+1} = (1-k_{i,n+1}^2)^{-1/2}\,(\underline{e}_{i,n} - k_{i,n+1}\underline{r}_{i-1,n})$$

$$\underline{r}_{i,n+1} = (1-k_{i,n+1}^2)^{-1/2}(\underline{r}_{i-1,n} - k_{i,n+1}\underline{e}_{i,n})$$

wherein

$$k_{i,n+1} = \langle \underline{e}_{i,n},\ \underline{r}_{i-1,n} \rangle$$

and $\langle\ \rangle$ represents an inner product. The symmetry of the recursion formulae is apparent. The equations are coupled by the term $k_{i,n+1}$ which is customarily called the "reflection coefficient." The estimate of the measurement (reference 10) at sample i for a model of order n is

$$\hat{y}_{i,n} = \sum_{j=0}^{n-1} \mathcal{E}\,(e_{i,j} \mid r_{i-1,j})$$

where $\mathcal{E}$ represents an orthogonal projection operator. Hence,

$$\hat{y}_{i,n} = [r_{n-1,0}, r_{n-1,1}, \ldots, r_{n-1,n-1}] \begin{bmatrix} k_{i,1} \\ k_{i,2} \\ \vdots \\ k_{i,n} \end{bmatrix}$$

so that

$$y_i = \Phi_L \cdot \Psi_i + \underline{e}_{i,n} \qquad (2)$$

where Φ_L is an orthonormal NS x n matrix $[\underline{r}_{n-1,0}, \ldots, \underline{r}_{n-1,n-1}]$ generated from the lattice filter, and ψ_i is the n dimensional vector of reflection coefficients and $\underline{e}_{i,n}$ is the NS dimensional estimation error vector.

Clearly, in this approach one may "fit the noise" by continually increasing the order of the system; however, once the order of the estimator has increased beyond the correct order, then the residual errors should lie within a noise band which can be predicted *a priori* based on assumed noise characteristics. A threshold value can be selected based on this predicted noise band and order determined by a test of whether or not the residuals have been reduced to lie within the noise band. The residuals will generally consist of signal and noise parts - the signal part being reduced as the correct order is reached until the residuals essentially consist only of noise. This test is carried out based on a data window of NW samples. Thus, assuming that the data can fit a linear model and that the noise process is Gaussian, for i large enough,

$$E\Big(\sum_{i=1}^{NW} \underline{e}_{i,n}^T\, \underline{e}_{i,n}\Big) = NW\ E(v_i v_i^T)$$

$$= NW\ \mathrm{tr}\ E(v_i v_i^T) = NW \sum_{j=1}^{NS} \sigma_j^2 \qquad (3)$$

where E is the expectation operator. This can be used as the one sigma threshold for the order determination test. In the last equation σ_j is the standard deviation of the noise process for the jth sensor. Reference 10 documents experience in choosing the data window size NW and the threshold level based on simulations.

ADAPTIVE CONTROL USING LATTICE FILTERS

Independent Modal Space Control (IMSC) (reference 11) is a control scheme specifically designed to deal with flexible spacecraft in a modal form amenable to control law design. Unfortunately, it requires natural modes and not the orthonormal basis provided by the lattice filter. Consequently, in order to interface the lattice filter outputs with the target adaptive control scheme (figure 1) and to make comparisons with finite element analysis predictions of natural modes, a method is needed to obtain natural mode shape estimates from the lattice filter basis. The filter updates the NM basis vectors at every sample instant. While the order estimate NM remains constant, the updated basis vectors are related by a mere rotational transformation. The assumption of the target adaptive control scheme is that the system motions can be modelled by a constant and finite set of natural modes and their associated modal amplitudes over a reasonably long time interval. Hence, when the estimated system order is constant, the basis elements used to derive the

model amplitude time series required by the target adaptive control scheme are not changed.

The transformation from the lattice filter to a natural mode basis should satisfy

$$\hat{y} = \phi_L \Psi_L = \phi_N \Psi_N$$

wherein the subscript L refers to the lattice filter and N refers to the natural modes. A non-singular matrix T, will satisfy this condition provided

$$\phi_L T = \phi_N \Psi_N = T \Psi_L \tag{4}$$

Since the order estimate is assumed constant, this matrix can be approximately determined on-line using the digital Fourier transform (DFT). Herein, this is accomplished as follows. Since the lattice filter uses the current measurement sample as its first basis element, the corresponding modal amplitude time series contains NM frequencies. Hence, the DFT spectrum of this series will contain NM peaks corresponding to these frequencies. The frequencies $(\omega_1, \omega_2, \ldots, \omega_{NM})$ can thus be identified by searching this spectrum for these peaks. Assuming that the motion is comprised of undamped structural vibrations, the matrix T, which produces the desired transformation can be calculated as

$$T = \begin{bmatrix} \mathrm{Re}[\Psi_L^1(\omega_1)] & \cdots & \mathrm{Re}[\Psi_L^1(\omega_{NM})] \\ \vdots & & \vdots \\ \mathrm{Re}[\Psi_L^{NM}(\omega_1)] & \cdots & \mathrm{Re}[\Psi_L^{NM}(\omega_{NM})] \end{bmatrix}$$

wherein, $[\psi_L^1(\omega), \ldots, \psi_L^{NM}(\omega)]$ is an NM dimensional vector of the modal amplitude transform. Using this matrix, the digital Fourier transform of each component of ψ_N will be zero at the discrete frequencies, ω_j, $j \neq i$. One item which degrades this approximation is the error in using DFT instead of the true Fourier transform. Still another is the assumption that the motion is made up of undamped structural oscillations. In spite of these items, reference 12 shows that this approach produces good estimates of the natural modes for the beam used herein.

The decoupled modal amplitude time series, $\Psi_N(i)$, as obtained above in equation (4), is then analyzed, for each mode, to identify the parameters of its autoregressive, moving average (ARMA) model. The inputs to each ARMA modal model are the generalized forces and hence, each model takes on the form:

$$\Psi_N(i) = A_1 \Psi_N(i-1) + A_2 \Psi_N(i-2) + B_1 f(i-1) + B_2 f(i-2) \tag{5}$$

where the f represents the generalized forces. Given the ψ_N and f's, the parameters A and B above are identified and used in the control law design process. Thus, the ARMA model output error is

$$e(i-1) = \Psi_N(i-1) - [\hat{A}_1(i-1)\Psi_N(i-2) + \hat{A}_2(i-1)\Psi_N(i-3) + \hat{B}_1(i-1)f(i-2) + \hat{B}_2(i-1)f(i-3)] \tag{6}$$

The gradient technique of reference 1 is used to identify the parameters $p = (A_i, B_i)$ using the iteration sequence

$$p(i) = p(i-1) + e(i-1)\,[W_1 \Psi_N(i-2),\ W_2 \Psi_N(i-3),\ W_3 f(i-2),\ W_4 f(i-3)] \tag{7}$$

As indicated in reference 1, the weights W must be selected consistent with the relation

$$W_1 \Psi_N^2(i-2) + W_2 \Psi_N^2(i-3) + W_3 f^2(i-2) + W_4 f^2(i-3) < 2$$

and the inputs to the algorithm, ψ_N and f, must be sufficiently varying and large if the parameters are to converge to their correct value.

For the identification and control scheme explained above to work satisfactorily in a closed loop environment, it is necessary to validate the design model. Three tests are suggested herein which check the following: 1) model fit error; 2) parameter convergence; and, 3) signal information. These tests have been used successfully in simulation and experimental work. The fit error test uses a fixed parameter set to calculate an estimated modal displacement for the past NT samples.

$$\sigma_{fit} > \sum_{n=0}^{NT} \Psi_N(i-n) - [\hat{A}_1 \psi_N(i-n-1) + \hat{A}_2 \psi_N(i-n-2) + \hat{B}_1 f_N(i-n-1) + \hat{B}_2 f(i-n-2)],\ k > NT$$

If the absolute sum of the error between the modelled displacement and the displacement calculated by the lattice filter exceeds a given threshold, the fixed parameter set is updated with the present identified parameter set. This process is repeated until the parameter set fits the data. The convergence test runs concurrently with the fit test. It simply checks the magnitude of the changes in successive estimated parameters.

$$\sigma_{conv} > \sum_{n=0}^{NT} |p_n - p_{n-1}| \quad \text{for } p^T = [\hat{A}_1, \hat{A}_2, \hat{B}_1, \hat{B}_2]$$

If the absolute sum of ten successive parameter estimates changes is above a specified level, a logical switch is set to indicate failure. The third and final test is on information content of the estimated modal amplitude signals from the lattice filters. The purpose of this test is to check whether enough information is present in the signal for proper identification of the parameters. If this test fails, the controller

gains are not updated based on the identified parameters, but are frozen at the last values before the test failed. Here, the estimated modal amplitudes and velocities from the lattice filter are checked for sufficient excitation by summing over ten samples.

$$\sigma_{inf} < \sum_{n=0}^{NT} |\psi_N| + |\psi_N - \psi_{N-1}|$$

The second term in the above equation represents a measure of velocity estimates. If the sum is below a threshold, σ_{inf}, the updating of the control gains based on the identified parameters is stopped. The information and fit error tests constitute one test for each mode and the convergence and reasonability tests constitute four tests for each mode. Thus, six tests must be passed before control is applied to a given mode. The actual stability and performance of the controller is directly affected by the criteria chosen for passing a test. If the test criteria are too stringent, system noise and nonlinearities may preclude initiation of control. However, if the tests are not adequate, it is possible that an error in the estimated parameters could result in gain calculations which produce an unstable system.

Now, consider the philosophy to be used when the tests described above pass or fail. When all the tests for parameters of a given mode have passed, control gains are calculated according to a previously developed pole placement scheme (reference 1). The control force commands are then calculated using these control gains. Considering the philosophy used when the tests fail, two cases were studied. In the first case, when the tests failed, control was turned off and the control forces were made zero. In the second case, when the tests failed, updating of the control gains was stopped and they were frozen at their values prior to the test failure. In this case, the control forces were not made zero and were computed using the frozen control gains. From a detailed study of both cases, it was found that the performance of the adaptive control system in the first case was superior to that of the second case.

APPLICATION TO A FLEXIBLE BEAM

The closed-loop adaptive control scheme of figure 1 has been tested in the digital simulation for the 12-foot, flexible free-free beam located at NASA Langley Research Center. The simulation contains the mathematical model of the beam apparatus in modal form. For this study, the simulation contains one rigid-body mode, the first three flexible modes, nine deflection sensors, and four actuators for control purposes. The initial conditions on the modal displacements were set to .05 in. and the modal velocities were set to zero. The modal damping was also set to zero. A digital sampling rate of 32 Hz was selected for the simulation, and the standard deviation for all measurement noise was assumed to be .005 based on observed noise in the available hardware. The lattice filter estimates were based on a data window size 4 (reference 10). The testing procedures were all carried out based on data window (NT) of ten samples. Initial parameters estimates were offset from the mathematically correct values to test and verify the rapid convergence of the identification algorithm. An arbitrary delay of 2 seconds was added between the time identification starts and when the control would be applied to show the behavior of the identification scheme.

At the start of the simulation, the lattice filter determines the number of modes in the simulation along with the mode shapes. Modal amplitude time histories are then generated. From the lattice filter mode shapes and modal amplitudes, natural modes and modal amplitudes are obtained through a linear transformation explained in the earlier section. The application of the transformation is delayed for 2 seconds because the online transformation technique of reference 12 requires 2 seconds of data for a digital Fourier transform data base to obtain the required transformation. The natural modal amplitudes are input to the equation-error parameter identifier which identifies the ARMA parameters. The identification results are then tested using the test procedures described above. When the tests are passed, the control is turned on. Results of the simulations are presented in figures 2-4.

Figure 2 shows the estimated modal displacement for the first lattice filter mode. The order estimate plot shows that the correct order of 4 is obtained in .3 seconds. After the parameter identification, when all the tests are passed, the control is turned on at 5.5 seconds and the modes are damped. The result of the adaptive control on the natural modes is shown in figure 3. It is evident that when the identification is validated by passing the tests and control turned on, the vibration suppression is achieved. When the modes are damped out the lattice filter order estimate drops from 4 to 1 indicating the flexible modes are damped out. Although the lattice filter order decreased, the control design order was maintained at 4 throughout the time interval when control was on. Allowing the order to vary in real time and updating the control order is a topic for further studies.

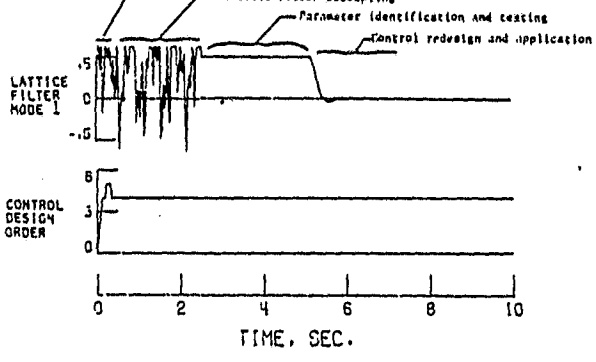

Figure 2.- Typical time history of an adaptive control run using identification, testing, and control design.

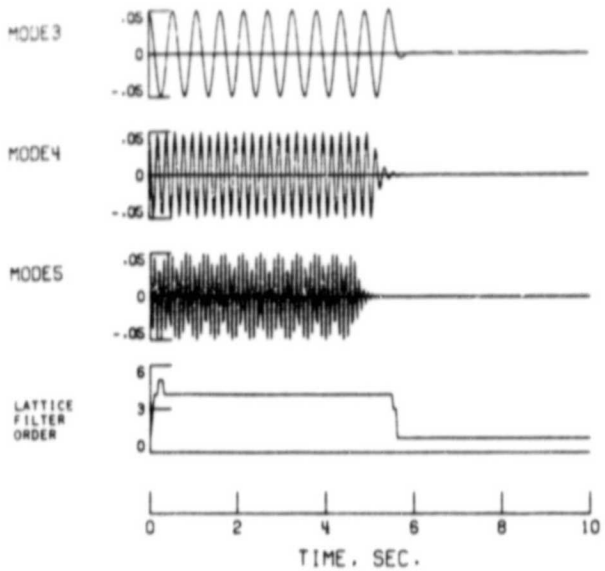

Figure 3.- Time histories of three natural modes with the lattice filter order indicated.

The main results of the identification and the test procedures are summarized in figure 4. For the first flexible mode, the figure shows the time histories of identified frequency parameter A_1 the fit error, a parameter that indicates algorithm convergence, and a parameter that indicates information content of the measurements. When all the tests are passed, the corresponding pass parameter (plotted as a binary logical varaible) is set to one. The various thresholds for the tests are also marked to indicate when the tests pass. These thresholds were determined based on detailed sensitivity studies of the modal control scheme for the beam (reference 13). An error was intentionlly put on the initial estimate of A_1 so that the convergence of the estimates to the correct value could be observed. When the identifier is turned on, the estimate converges to the true value of 1.8 from 3. The thresholds indicate that the fit error test is passed first and then the convergence test. With enough signal in the measurements the information test is always passed. When all the tests are passed at 5.5 sec, the control is turned on. When control is fully effective, that is when the modes are damped out, the measurement data will contain only the noise and the information test will fail. This is immediately seen from the history of A_1 as it starts oscillating with large amplitude indicating that the modal amplitude signal contains mainly noise. Also, if the parameter excursions are large, the convergence tests will also fail indicating a failure for the binary variable pass. Once this happens, the control gain updating is stopped, and control forces were made zero.

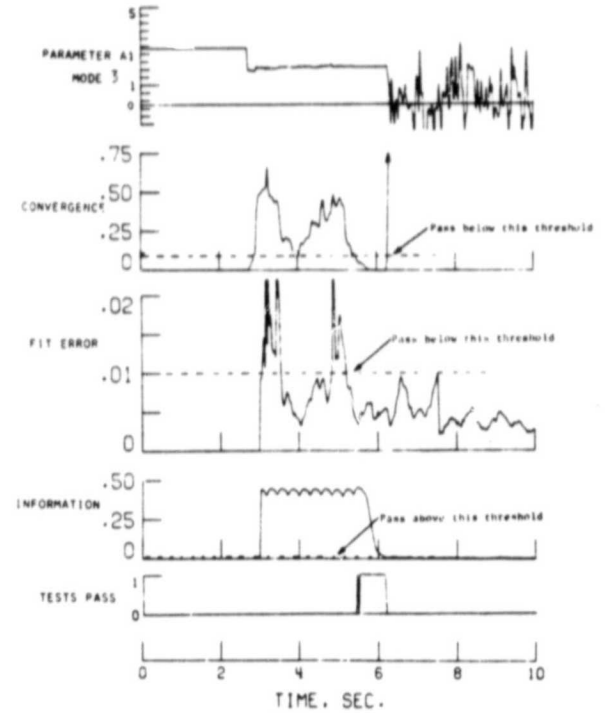

Figure 4.- Time histories of the test variables for one mode with the test thresholds and logic sum of the tests indicated.

PROBLEMS IN PRACTICAL IMPLEMENTATION

The adaptive control scheme of figure 1 is good from the engineering point of view since only validated models are used for control system design. A natural question arises as to the course of action when validation tests fail. The operating environment for large flexible spacecraft is, fortunately, benign and a system designed to suppress vibrations can be shut down at the expense of having to conduct relatively long term maneuvers. Another saving feature of large flexible spacecraft is that collocated rate feedback is stable and relaxation of the system to this mode of operation is also possible, again, with corresponding degradation in performance. Therefore, two options that can be evoked are; one, to shut down the control system and the other, to revert to a robust control system design which insures stability.

At first glance one may wish to use the ARMA model generated by the lattice filter directly in the design process rather than using IMSC with its requirement of generating natural modes. Unfortunately , the current online design capability for controllers of vector ARMA processes is not adequate. Having selected IMSC, one must obtain natural modes from the vector ARMA model or from the measurement time series. Here the same problem arises, that is, the current capability of eigenvalue/vector analysis for vector ARMA processes is inadequate for online implementation. Hence, a time series analysis using a DFT has been selected. The accuracy of the process of extracting natural modes is directly affected by the number of data points processed. Hence, there is a tradeoff to be made between the higher

complexity in control computations versus the error in the natural modes using the DFT approach. Also, significant computational saving results if the approximation of zero damping can be evoked. If this approximation cannot be made, then one must work with complex modes.

Since several approximations are required by the system, a method of validating the models used in the online controller design is essential. Analytic methods of validating models based on statistical error analysis (e.g. Cramer-Rao bounds) are not adequate. Currently, tests on fit error, algorithm convergence, information content of the measurements, and reasonability have been used. The thresholds and design constants for these tests can be determined only by exhaustive simulation and/or hardware tests and is not an online procedure.

CONCLUSION

This paper reviews the use of the least square lattice filter in adaptive control systems. Emphasis is placed on the integration of the lattice filter into a practical parameter adaptive control system. One novel feature of the recommended system is the inclusion of a design model validation scheme based on model fit error, algorithm convergence, and signal information content. An application is presented for adaptive control of a flexible beam. These results indicate that the lattice filter adaptive scheme is practical for vibration control of large flexible spacecraft. Difficulties in the practical implementation of the lattice filter in adaptive control are also discussed. These centered around the computational burden of transforming lattice filter modes into natural modes and the selection of the thresholds for online validation tests.

REFERENCES

1. Johnson, C. R. and Montgomery, R. C.: A Distributed System Adaptive Control Strategy. IEEE Trans. on Aerospace and Electronic Systems, Vol.-AES-15, No. 5, 1979, pp. 601-612.

2. IEEE Trans. on Acoustics, Speech and Signal Processing, Special Issue on Adaptive Signal Processing, Vol. ASSP-29, No. 3, June 1981.

3. Friedlander, B.: Lattice Filters for Adaptive Processing. Proc. of IEEE, Vol. 70, No. 8, August 1982, pp. 829-867.

4. Friedlander, B.: Recursive Lattice Forms for Adaptive Control. Proc. JACC, San Francisco, California, 1980.

5. Martin-Sanchez. J.: A New Solution to Adaptive Control. Proc. IEEE, Vol. 64, No. 8, August 1976, pp. 1209-1218.

6. Widrow, B., McCool, J. M. and Medoff, B. P.: Adaptive Control by Inverse Modelling. Proc. of 12 ASILOMAR Conference on Circuits, Systems and Signal Processing, 1978, pp. 90-94.

7. Olcer, S. and Morf, M.: Adaptive Control by Ladder Forms. Proc. of American Control Conference, June 1984, San Diego, pp. 1265-1270.

8. Shah, S. C., Walker, R. A. and Saberi, H. A.: Multivariable Adaptive Control Algorithms and Their Mechanizations for Aerospace Applications. Proc. of IEEE Conference on Decision and Control, Las Vegas, Nevada, December 1984, pp. 381-386.

9. Sundararajan, N., Williams, J. P. and Montgomery, R. C.: Adaptive Modal Control of Structural Dynamics Systems Using Recursive Lattice Filters. J. of Guidance, Control and Dynamics, Vol. 8, No. 2, 1985, pp. 223-229.

10. Sundararajan, N., and Montgomery, R. C.: Identification of Structural Dynamics System Using Least Square Lattice Filters. Journal of Guidance, Control and Dynamics, Vol. 6, No. 5, September-October 1983, pp. 374-381.

11. Meirovitch, L. and Oz, H.: Modal Space Con rol of Distributed Gyroscopic Systems. Journal of Guidance and Control, Vol. 3, No. 2, January-February 1980, pp.140-150.

12. Sundararajan, N., Montgomery, R. C.: Decoupling the Structural Mode Estimated Using Recursive Lattice Filters. Proceedings of the 21st IEEE Conference on Decision and Control, December 1982, pp.998-999.

13. Williams, J. P. and Montgomery, R. C.: Simulation and Testing of Digital Control on a Flexible Beam. Proceedings of the AIAA Guidance and Control Conference, August 1982, pp. 403-409.

APPENDIX D

ROBUST CONTROLLER SYNTHESIS FOR A LARGE FLEXIBLE SPACE ANTENNA

ROBUST CONTROLLER SYNTHESIS FOR A LARGE FLEXIBLE SPACE ANTENNA

N. Sundararajan*, S. M. Joshi, and E. S. Armstrong
NASA-Langley Research Center
Hampton, Virginia 23665

SUMMARY

This paper investigates the application of the linear-quadratic-Gaussian (LQG)/ loop transfer recovery (LTR) method to the problem of synthesizing a fine-pointing control system for a large flexible space antenna. The LQG/LTR approach of synthesizing a multivariable controller in the frequency domain is selected because large flexible structures can be modelled with elastic mode transfer functions as additive perturbations on the rigid body model and the LQG/LTR approach uses this formulation naturally for robust control design. The study is based on a finite element model of the 122 m Hoop/Column antenna, which consists of three rigid-body rotational modes and the first ten elastic modes. A robust compensator design for achieving the required pointing performance in the presence of modeling uncertainties is obtained using the LQG/LTR method. For the Hoop/Column antenna, a satisfactory controller design meeting the desired bandwith of .1 rad/sec and ensuring stability with unmodelled high frequency modes was obtained using only a colocated pair of 3-axis attitude sensors and torque actuators. This study also indicates that to achieve the desired performance bandwidth of 0.1 rad/sec. and to ensure stability against higher frequency elastic modes, the design model should include the first three flexible modes together with the rigid body modes.

---

* Old Dominion University Research Foundation, Norfolk, VA

INTRODUCTION

One of the planned activities of the NASA's Space Transportation System is the placement in earth orbit of a variety of large space antennas. Potential space missions will require antennas and structures ranging from 30m to 20km in size. Applications include communications (mobile), remote sensing (soil moisture, salinity, etc.), deep space network (orbital relays), astronomy (x-ray, observatory, optical array, radio telescope, very long baseline interferometry, etc.), energy and space platforms. Specific missions have been pinpointed and future requirements have been identified for large space antennas for communications, earth sensing and radio astronomy [1]. Particular emphasis is placed on mesh-deployable antennas in the 50-120 meter diameter category. One such antenna is the Maypole (Hoop/Column) antenna, shown schematically in Figure 1, basically consisting of a deployable central mast attached to a deployable hoop by cables held in tension [2]. The deployable mast consists of a number of telescoping sections, and the hoop consists of 48 rigid segments. The reflective mesh, which is made of knit gold-plated molybdenum wire, is attached to the hoop by graphite fibers. The mesh is shaped using a network of stringers and ties to form the radio frequency (RF) reflective surface. In order to achieve required RF performance, the antenna must be controlled to specified precision in attitude and shape. For example, for missions such as land mobile satellite system (LMSS), which is a communication concept for providing mobile telephone service to users in the continental United States, it is necessary to achieve a pointing accuracy of 0.03 degree RMS (root mean square) and a surface accuracy of 6 mm RMS. It is also necessary to

have stringent control on the motion of the feed (located near one end of the mast) relative to the mesh. Because of its large size and relatively light weight, the antenna is highly flexible, with a large number of significant elastic modes. Its dynamics can be represented by partial differential equations, or by very large systems of ordinary differential equations. The resulting equations have many resonant frequencies, some of which may be very low, and possibly closely spaced. The natural damping is usually very small. For these reasons, control of large space structures is a challenging task [3]. Since the system is inherently of high order, a practical controller has to be based on a reduced-order "design" model. Furthermore, the parameters (i.e., frequencies, mode shapes, and damping ratios) of the system are known imprecisely. This introduces additional modeling errors. Typically, the modeling errors for finite element models increase substantially with increasing modal frequency.

Reduced-order control synthesis for the Hoop/Column antenna using the standard LQG theory was investigated in [4,5]. The standard LQG procedure yielded satisfactory control, i.e., rigid-body bandwidth of up to 0.25 rad/sec, satisfactory time constants for the elastic modes, and acceptable root mean square (RMS) pointing errors in the presence of sensor noise. It should be noted that the LQG approach in reference 4 used a large number of actuators and sensors (four 3-axis torque actuators and four 3-axis attitude and rate sensors). It was found in [4] that the first three flexible modes had to be included in the "design" model (in addition

to the three rigid modes) to obtain satisfactory performance. The main problem with the LQG method was that a large number of weighting parameters had to be simultaneously adjusted to obtain a good design. In addition, the stability robustness property with respect to inaccuracies in the modal parameters could not be properly evaluated because it was difficult to effectively characterize the bounds on modeling errors in a time-domain setting. In order to reduce these difficulties, normally one checks the control design for robustness after the control design is completed using LQG or any other method. Such an approach in the frequency domain using singular value measures was presented in [6] for a large space structure using different control design methods like LQG, integral feedback, 'frequency shaped' LQG, etc. Unlike the above methods, the LQG/LTR approach provides a means of including the robustness-to-uncertainities, in the control design process itself. Since it is in the frequency domain, it extends the basic frequency domain design guidelines like bandwith, cross-over frequency, etc. from a scalar system to a multivariable system.

The newly emerging robust control synthesis methodology which uses frequency domain matrix norm bounds (i.e., singular values) has received considerable attention in the recent literature [7-9]. The basic framework for frequency domain synthesis using the LQG/LTR methodology was developed in [7-9]. It has been applied to diverse systems such as power systems [10] and aircraft engine control [11]. The LQG/LTR design philosophy uses a low-frequency "design model" of the plant and a

high-frequency characterization of the modeling errors. This method, which characterizes unstructured uncertainty with singular value bounds, appears to be particularly well suited for the control of large flexible spacecraft due to the considerable uncertainty that inherently exists in the mathematical models.

The purpose of this paper is to investigate the use of LQG/LTR multivariable frequency domain methodology in the design of an attitude control system for the Hoop/Column antenna. A low order compensator is obtained by treating a sequence of finite element design models ordered with increasing modal frequency and choosing the final design model as the first one which allows the performance/robustness objectives to be met. In this sequence of design models, the first one consists of the rigid body modes only. Subsequent design models are obtained by the successive addition of flexible modes. The designs use 3-axis torque actuators, colocated attitude sensors, and attitude feedback.

The organization of this paper is as follows: The mathematical model of the system is described in section 2. The control objective is briefly discussed in section 3, followed by a brief description of the LQG/LTR technique in section 4. The reduced order (low frequency) design model and the high frequency model uncertainty barrier are also discussed in this section. Section 5 presents the results of synthesizing the controller based on the above procedure using only attitude feedback. Some of the problems and limitations observed are also highlighted. Based on the study results, the conclusions are summarized in section 6.

2. MATHEMATICAL MODEL

As a consequence of its large size and light weight, the Hoop/Column antenna is a highly flexible system having a large number of significant structural modes. A finite element model of the antenna [Ref. 2] is used in this paper. The mathematical model considered consists of rotational rigid-body dynamics (about the three axes) and the elastic motion. We assume that the control will be accomplished by using n_T three-axis torque actuators. The linearized equations of motion are:

$$I_s \ddot{\alpha} = \sum_{j=1}^{n_T} T_j \tag{1}$$

$$\ddot{q} + D\dot{q} + \Lambda q = \Phi^T u \tag{2}$$

where I_s is the 3 x 3 inertia matrix, T_j is the 3-axis torque applied by the jth actuator, $\alpha_s = (\phi_s, \theta_s, \psi_s)^T$ denotes the rigid-body attitude, q is the n_q x 1 modal amplitude vector (for n_q structural modes), $D = 2\,\mathrm{diag}(\rho_1\omega_1, \rho_2\omega_2, \ldots, \rho_n\omega_n)$ is the inherent damping matrix, (where ρ_i is the damping ratio for the ith mode). Φ is the m x n_q "mode-slope" matrix (where $m = 3n_T$), $u = (T_1^T, T_2^T, \ldots, T_{n_T}^T)^T$ is the m x 1 vector of actuator torques, and $\Lambda = \mathrm{diag}(\omega_1^2, \omega_2^2, \ldots, \omega_{n_q}^2)$ where ω_i is the frequency of the ith elastic mode. The rigid-body parameters and the first ten elastic frequencies are given in Table 1. Each value of ρ_i is assumed to be 0.01 for i=1,2, ...,n .

Normally, the sensors used include attitude and rate sensors. A 3-axis attitude y_a at a sensor (e.g. a star tracker) output is given by:

$$y_a = \alpha_s + \psi q + w \tag{3}$$

where ψ is the 3 x n_q mode-slope matrix at the sensor location, and w is the sensor noise. If an attitude rate sensor (e.g. a rate gyro) is used, the sensor output y_r is given by an equation similar to (3), except that α_s and q are replaced by $\dot{\alpha}_s$ and $\dot{q}$, respectively. Torque actuators and attitude sensors are assumed to be located near the top of the mast at the antenna feed (Fig. 1.)

Defining $x = (\alpha_s^T, \dot{\alpha}_s^T, q^T, \dot{q}^T)^T$ an n x 1 vector, the state space model can be written in the form:

$$\dot{x} = A_F x + B_F u \tag{4}$$

$$y = C_F x + w \tag{5}$$

The sensor noise w is not used in the design process in this paper; however, it will have to be included when computing the RMS pointing errors. Ignoring the noise, the transfer matrix between the input (3-axis torque) and the output (3-axis attitude) is given by:

$$G(s) = G_1(s) + G_2(s) \tag{6}$$

where

$$G_1(s) = I_s^{-1}/s^2 \tag{7}$$

$$G_2(s) = \sum_{i=1}^{n_q} (\psi_i \phi_i^T)/(s^2 + 2\rho_i \omega_i s + \omega_i^2) \tag{8}$$

(ψ_i and ϕ_i represent the mode-slope matrices at the sensor and actuator locations corresponding to the ith mode).

3. DESIGN OBJECTIVES

The basic design objectives for the control systems are: (1) To obtain sufficiently high bandwidth (i.e. closed loop frequencies corresponding to the rigid body modes) and satisfactory closed loop damping ratios for the rigid body and structural modes; and (2) To obtain satisfactory RMS pointing errors, feed motion errors and surface errors. The first design objective arises from the need to obtain sufficiently fast error delay when a step disturbance(such as sudden thermal distortion caused by entering or leaving Earth's shadow) occurs. The second design objective arises from the RF performance requirements. These two objectives may not necessarily be compatible, and may even be conflicting. For example, the use of increased feedback gains for obtaining higher bandwith and damping ratios will, in general, result in higher r.m.s errors (because of the amplified effect of sensor noise) beyond a certain point. Therefore, it is necessary to carefully consider the trade-offs between the speed of response and lower RMS error. In this study, the main control system specification is that a minimum bandwith of

0.1 rad/sec for the closed loop system is to be ensured. The upper limit on the low frequency gain is not specified, but it is desired that it should be as high as possible. Also, for this study no specification on RMS errors was made and this aspect along with measurement noise will be considered in the future.

4. THE DESIGN PROCEDURE

The LQG/LTR method has been described in detail in [7-9]. Here, the main steps are summarized first and then each step is discussed in detail.

(1) Define a "design" model of the nominal plant which is an acceptable low frequency representation. Define the high frequency uncertainty (robustness) barrier, and the low frequency performance barrier.

(2) Design a full state feedback compensator based on the steady state Kalman-Bucy filter (KBF). This assumes that the loop is broken at the output. Adjust the weighting matrices in the KBF design until its frequency response meets the robustness specifications at high frequencies and bandwidth specification at low frequencies.

(3) Design a LQ regulator to asymptotically "recover" the frequency response obtained in step 2.

(4) Verify stability, robustness, and performance for the entire closed-loop system.

The first step, which consists of the definition of the plant and the uncertainty (robustness) barrier, is often the most important one. The basic problem in controlling a flexible structure is the presence of a

large number of lightly damped structural modes. Practical limitations necessitate the use of reduced-order controllers. Therefore, the uncontrolled modes, as well as the error in the knowledge of the controlled modes, represent uncertainty. Since the number of structural modes is usually large and finite element modeling accuracy typically decreases with increasing model frequency, the design model should consist of the rigid-body plus the first few elastic modes. The remaining structural modes then (partly) constitute the plant uncertainty. In order to obtain an acceptable low-frequency representation, the design model must include at least the three rigid body modes. The uncertainty barrier is a measure of the plant uncertainty at high frequencies. The plant uncertainty can be represented as either multiplicative or additive uncertainty (Fig. 2). Additive uncertainties are of the form

$$G' = G + \Delta G$$

while multiplicative uncertainties are of the form

$$G' = (I+\Delta)G$$

Multiplicative uncertainty form is the preferred form in the literature on robustness studies as the compensated transfer function has the same uncertainty representation as the raw model. However, since flexible structure models exhibit naturally the additive uncertainty form of the transfer function matrix, this will be used in the following studies. The LQG/LTR approach requires the characterization of the uncertainty in terms

of a frequency-dependent upper bound. Frequency domain sufficient conditions are used to test the robustness in the presence of uncertainties within that bound.

For the case of multiplicative uncertainty $L_p(s)$ of figure 2a, the closed-loop system is stable if

$$\bar{\sigma}[L_p(j\omega)-I] \leq \underline{\sigma}\,[I + (G_p(j\omega)G_c(j\omega))^{-1}] \tag{9}$$

where $G_p(s)$ and $G_c(s)$ are the design model (plant) and compensator transfer matrices, and $\bar{\sigma}$ and $\underline{\sigma}$ denote the largest and the smallest singular values of the argument matrix, respectively. At high frequencies, assuming $\|[L_p(j\omega)]\| \gg 1$ and $\|[G_p(j\omega)G_c(j\omega)]\| \ll 1$, (9) approximately yields

$$\bar{\sigma}\,(G_pG_c) \quad < \quad \frac{1}{\bar{\sigma}\,(L_p)} \tag{10}$$

The "uncertainty (or robustness) barrier" is an upper bound $l_m(\omega)$ on $\sigma(L_p)$. The system is stable in the presence of such unstructured uncertainties if $\sigma[G_pG_c] < l_m^{-1}(\omega)$ at high frequencies.

When the additive uncertainty formulation (Fig. 2b) is used, a sufficient condition for stability robustness is given by [12]

$$\frac{\underline{\sigma}\,(I + G_pG_c)}{\bar{\sigma}(G_c)} \quad > \quad \bar{\sigma}\,(\Delta G) \tag{11}$$

At high frequencies, assuming $\|G_pG_c\| \ll 1$, (11) (approximately) yields

$$\bar{\sigma}(G_c) \quad < \quad 1/\bar{\sigma}(\Delta G) \tag{12}$$

That is, the compensator must roll off sufficiently rapidly at high frequencies. The main objective of the LQG/LTR approach is to first design a full state compensator (based on KBF) which has the behavior of the desired loop transfer matrix (i.e., the loop gain G_pG_c). Therefore, (from step 2) any loop shaping should involve the product G_pG_c rather than G_c alone as in (11) and (12). Assuming that G_p is a square matrix,

$$G_c = G_p^{-1}(G_p\, G_c) \tag{13}$$

$$\bar{\sigma}(G_c) < \bar{\sigma}(G_p^{-1})\,\bar{\sigma}(G_p\, G_c)$$

or

$$\bar{\sigma}(G_c) \quad < \quad \bar{\sigma}(G_p^{-1})\,\bar{\sigma}(G_pG_c) \tag{14}$$

Using (12) and (11), the following sufficient condition for stability robustness is obtained:

$$\frac{\underline{\sigma}(I + G_pG_c)\,\underline{\sigma}(G_p)}{\bar{\sigma}(G_pG_c)} \quad > \quad \bar{\sigma}(\Delta G) \tag{15}$$

The second step in the design procedure is to design a full state feedback compensator having desirable singular value properties. The

performance of the closed-loop system depends on the low frequency gain and the crossover frequency of the loop transfer matrix G_pG_c; that is, on the behavior of $\underline{\sigma}\ [G_pG_c]$. Larger low frequency gain and crossover frequency indicates better tracking performance. Thus, $\underline{\sigma}[G_pG_c]$ should lie above the performance specification as shown in Fig. 3a. The other requirement is the stability robustness in the presence of model uncertainties. If the multiplicative uncertainty formulation is used, according to (10), the $\bar{\sigma}\ [G_pG_c]$ plot should pass under the robustness barrier $\bar{\sigma}^{-1}(L_p)$ at high frequencies (Fig. 3a). On the other hand, if the additive formulation is used, the robustness condition (15) should be satisfied (Fig. 3b). The advantage of an LQG-based full state design is that it has excellent classical properties, and its frequency response can be shaped in the desired manner by varying the weighting matrices [8]. As discussed in [7], this design can be accomplished using the LQR Riccati equation if the loop is broken at the plant input, or the KBF Riccati equation if it is broken at the point where the residual signal enters the KBF. Herein we select the latter because the objective is to control the attitude output. This selection is also consistent with [9-11]. The KBF equations are:

$$A\Sigma + \Sigma A^T + LL^T - \frac{1}{\mu}\Sigma C\ C^T\Sigma \quad = 0 \tag{16}$$

$$H = \frac{1}{\mu}\Sigma C^T \tag{17}$$

where L and μ are the design parameters, L being an μ x m matrix, and μ a scalar. The matrix H is the KBF gain and Σ is the corresponding Riccati matrix. The KBF loop transfer matrix is given by:

$$G_{KF}(s) = C\,(sI - A)^{-1}H \tag{18}$$

Generally, the frequency response $\sigma(G_{KF}(j\omega))$ would shift higher as μ decreases, and the crossover frequency can be adjusted by changing L [6].

Having obtained satisfactory singular value behavior of KBF, the next step is to design a LQR to "recover" the desired frequency response. This is accomplished by solving the algebraic Riccati equation

$$A^TP + PA^T - PBB^TP + q\,C^TC = 0 \tag{19}$$

where P is the Riccati matrix and q is a positive scalar. The control gain matrix G is given by

$$G = R^{-1}B^TP$$

It has been proven in references 7 and 8 that the loop transfer matrix G_pG_c for the overall system (consisting of the plant, the KBF and the LQR) tends to $G_{KF}(s)$ as $q\to\infty$, provided that the open-loop plant has no transmission zeros in the right half plane. The compensator $G_c(s)$ after recovery is given by:

$$G_c(s) = G\,(sI - A + BG + HC)^{-1}H$$

Since the compensation obtained has no guaranteed robustness properties, the last step will consist of testing the eigenvalues of the entire closed-loop system to ensure stability and robustness. If instability is discovered, it will be necessary to return to step 2 and redesign the KBF for lower bandwidth and the LQR for robustness recovery. If this does not produce satisfactory results, it would then be necessary to return to step 1 and include more elastic modes in the design model. Application of the foregoing LQG/LTR procedure for the Hoop/Column antenna is described in the following section.

5. CONTROLLER DESIGN BY LQG/LTR METHOD USING ATTITUDE FEEDBACK

The foregoing procedure has been applied to the Hoop/Column antenna model. The computations of singular values of various matrices (e.g. loop transfer, return difference, inverse return difference matrices) were carried out using a recently developed multivarable frequency domain analysis software package (FREQ), and the LQG designs were carried out using ORACLS [13]. The nominal plant includes three rotational rigid-body modes and the first ten elastic modes. We assume three torque actuators; hence, the order of B matrix is 26x3. Assuming three attitude sensors (one for each axis) at the same location as the actuators, C is a 3 x 26 matrix. The plant, input, and output matrices were obtained from a finite element analysis of the antenna.

Before starting the controller design, the maximum and minimum singular values ($\bar{\sigma}$ and $\underline{\sigma}$) of the full, nominal, open-loop plant transfer matrix were obtained and are shown in figure 4. The g plot clearly shows the peaks at the elastic mode frequencies (i.e. the poles), the most prominent being the first mode near .75 rad/sec. The dips in $\underline{\sigma}$ indicate the presence of transmission zeros for the multivariable plant at those frequencies. The controller synthesis studies are performed using the design model consisting of:

a) rigid-body model ($n = 6$, $n_q = 0$)

b) rigid-body and the first flexible mode ($n = 8$, $n_q = 1$)

c) rigid-body and the first three flexible modes ($n = 12$, $n_q = 3$)

The measurements available are the three attitude angles at the feed location. One 3-axis torque actuator is used at the same location. The compensator is designed based on these sensors and actuators.

5.1 Rigid Body Model:

In this section the controller design is carried out based only on the rigid body design model. The largest and the smallest singular values of the rigid-body transfer matrix ($n = 6$) are of the form $1/s^2$. The corresponding additive uncertainty ΔG, which consists of the (20th order) flexible dynamics, is plotted in figure 5. Figure 5 indicates the presence of poles at the undamped flexible mode frequencies of 0.75 rad/sec, 1.35 rad/sec, etc. Also, the pole of the first mode frequency of 0.75 rad/sec produces the highest peak since it is most lightly damped.

(The importance of this fact will be seen later when the stability condition is violated at this point).

For this sixth order design model, a compensator design was carried out using the Kalman filter design methodology to achieve satisfactory performance (i.e., large gain and bandwidth) at low frequencies, and robustness at high frequencies. This design was carried out using the Kalman filter Riccati equation (16). The Kalman-Bucy filter (KBF) transfer matrix $G_{KF}(s)$ is given in equation (18). Appropriate loop-shaping can be accomplished by proper choice of the weights μ and L in equation (16). Since the controller design model is of the form $1/s^2$, one can analytically evaluate the singular values of $I+G_{KF}$ using equations (16) and (17). Assuming $\mu = 1$ and $L = (L_1, L_2)^t$ the left hand side of (15) can be solved. For $L_1 = 0$ and $L_2 = k_2 I$, it can be shown that equation (15) is satisfied by:

$$k_2 < 10^{-7}$$

This implies that the Kalman filter gain computed using (17) will be very low. Figure 5 shows plots for condition (15) with two L matrices, with $L_1 = 0$ and $k_2 = 10^{-6}$ and 10^{-7}. The right hand side of (15) is also plotted in figure 5. It is evident that condition (15) is satisfied for $k_2 = 10^{-7}$. As k_2 is decreased further, the curve shifts upward thus increasing the margin.

The next step consists of LQ regulator design. Having obtained an acceptable compensator through Kalman-Bucy filter equations, the LQ regulator is realized via the loop transfer recovery method [8]. Figure 6 presents the singular value plots of the complete loop transfer matrix $G_p G_c(s)$ (which consists of the plant, the KBF and the LQR) for different weighting parameter q (Eq. 19). The q selected was $q=10^6$ and 10^7. It is easy to check condition (11) in this case. As q is increased, the plots approach those of the compensator obtained from the Kalman filter design approach. The LQ design for $q=10^6$ was considered to be satisfactory.

The standard LQG/LTR procedure requires the definition of the "desired" loop transfer characteristics (see step two in section three.) That is, $\underline{\sigma}(G_{KF})$ must satisfy the low-frequency performance specifications, and $\bar{\sigma}(G_{KF})$ must satisfy the high-frequency robustness specifications. Thus, in the presence of additive uncertainty ΔG, the procedure states that the robustness condition

$$\frac{\underline{\sigma}(I + G_{KF})\,\underline{\sigma}(G_p)}{\bar{\sigma}(G_{KF})} > \bar{\sigma}(\Delta G)$$

should be satisfied. However, in the case described above, it was found that the above condition makes the "desired" design (G_{KF}) extremely conservative. From figure 6, it is seen that the closed loop bandwith is quite low and nowhere near the desired value of .1 rad/sec. Therefore,

recovering this conservative loop gain yields a compensator with poor performance. This fact led to a modification of the LQG/LTR procedure. In particular, the above robustness test on G_{KF} is omitted in the modified procedure. Instead, the recovery is carried out first, and then the (less conservative) stability test (11) is applied directly for the compensator G_c. The Kalman filter transfer matrix G_{KF} is based only on the desired performance and not on satisfying the stability test of equation (15).

With the revised test on G_c, the following choices on L and μ matrices were made.

$$L = \begin{bmatrix} 0 \\ - - - - \\ 10^{-2}I \end{bmatrix} \quad ; \mu = 1$$

Using the recovery procedure, the compensator is obtained for this case wth $q = 10^4$. The resulting stability test (Eq. 11) is shown in figure 7. It is seen that the stability margin is lowest at the first mode frequency (0.75 rad/sec). Any increase in the gain (obtained by $q > 10^4$) resulted in violation of stability condition at that point. The overall loop bandwidth is obtained from the singular values of the loop transfer function G_pG_c shown in figure 8. It is seen that the bandwidth (i.e., the frequency at which $\underline{\sigma}(G_pG_c) = 1$) is far short of the required 0.1 rad/sec. In order to increase the bandwidth, the gain

has to be increased by increasing q. However, this results in the violation of the stability condition (11). Thus it is evident that, with a rigid-body design model, it is not possible to meet the performance specifications.

5.2 1 Flexible Mode Design Model:

To overcome the above problems, the next alternative that was considered was whether the inclusion of the first flexible mode (0.75 rad/sec) in the design model would improve the performance. The inclusion of the first flexible mode, which is predominantly a torsion mode, results in a design model of order 8. The singular values of ΔG shown in figure 9 are an order of magnitude lower than those in figure 5 (wherein ΔG consisted of all the flexible modes). The first peak of $\sigma(\Delta G)$ occurs at 1.35 rad/sec, which is the frequency of the second mode. This is the critical point in the stability test (Eq. 11). After a number of trials, the following choice of L and μ was made to obtain the desired performance G_{KF}.

$$L = \begin{bmatrix} 0 \\ \hline 10^{-1}I_3 \\ \hline 10^{-1}I_2 \mid 0 \end{bmatrix} ; \mu = 1$$

The recovery is obtained for $q = 10^5$ and the stability test is shown in figure 9. Fig. 9 indicates the critical point to be at about 0.28

rad/sec. There is a good margin at the peaks of ΔG due to upward sloping of the upper curve. The resulting loop transfer function ($G_p G_c$) plots are shown in figure 10. The plots indicate that the required 0.1 rad/sec bandwidth is not obtained (although it is much higher than the rigid-model case). Any increase in the gain (for $q > 10^5$) was found to result in the violation of the stability condition (11). Figure 10 indicates the presence of an open-loop invariant zero near 0.082 rad/sec, which was also confirmed by independent computations. This zero is almost on the imaginary axis (i.e., the transfer matrix is close to being nonminimum phase). Therefore, (as would be expected) the recovery procedure is not very effective for making $G_p G_c$ approximate G_{KF}.

5.3 3 Flexible Mode Model:

In order to improve the performance further, the next step was to include the first three flexible modes in the design model. It is logical to do this because they represent the first modes about each axis, i.e., the first torsion mode, and the first bending modes in the XZ and YZ planes. Thus, the order of the design model was 12. The singular value plots for G_p and ΔG are shown in figures 11 and 12, respectively. It is seen from figure 11 that G_p has zeros near 0.082 and 0.22 rad/sec, and poles near 0.75, 1.35, and 1.7 rad/sec. It is seen from the ΔG plot (Fig. 12) that $\bar{\sigma}$ is considerably lower than that in figures 7 and 9. After numerous trials, the following choice of the L matrix and the scalar μ was made for a suitable G_{KF}:

$$L = \begin{bmatrix} 0 \\ \hline 10^{-1}I_3 \\ \hline 10^{-4}I_2 \;\vdots\; 0 \\ \hline 10^{-4}I_2 \;\vdots\; 0 \\ \hline 10^{-4}I_2 \;\vdots\; 0 \end{bmatrix} \qquad ; \mu = 1$$

The recovery was accomplished with $q = 10^{10}$. The stability test is shown in figure 12. It can be seen that condition (11) is satisfied with a wide margin. Also, at the peak for ΔG (at 8 rad/sec) the upper curve slopes upward, indicating good tolerance of high-frequency uncertainty. The limit for increasing the gain (indicated by the lowest point in the upper curve in figure (12) occurs at about 0.3 rad/sec. The resulting compensator G_c is shown in figure 13. The gain of G_c is much higher than that obtained in the previous cases. Generally, the LQG/LTR technique attempts to choose G_c in such a way that the product G_pG_c is replaced by G_{KF} (i.e. G_c is attempting to invert G_p in the frequency range of interest). The 3-mode design plant shown in figure 11 has elastic mode eigenvalues at $-.0075 \pm j.75$, $-.0135 \pm j1.35$, and $-.0170 \pm j1.70$. Figure 13 shows that G_c has zeros with frequencies near these locations. The design plant also has transmission zeros at $-.9 \times 10^{-4} \pm j.082$, $-.37 \times 10^{-3} \pm j.22$, and $-.29 \times 10^{-3} \pm j.22$. Ideally, G_c should have poles with frequencies near .082 and .22. However, the design

plant zeros are too near the $j\omega$-axis and tend to numerically behave as nonminimum phase. Some attenuation is obtained by the compensator pole near .4 rad/sec. The plots for the loop transfer matrix G_pG_c are given in figure 14. It is seen that a bandwidth of 0.1 rad/sec. is obtained except for the presence of the invariant zero near 0.082 rad/sec. which causes some deterioration of performance. At frequencies past .4 rad/sec., G_pG_c behaves like G_{KF} and eventually rolls off at 60db/decade. Also, $\underline{\sigma}$ and $\bar{\sigma}$ are closely spaced, indicating good system behavior. Thus it is seen that the inclusion of the first three modes in the design model yields a robust compensator which also meets the bandwidth specifications.

The final step is to check the stability of the complete nominal system when the compensator $G_c(s)$ designed above is used. The overall closed-loop system is:

$$\begin{bmatrix} \dot{x} \\ \dot{\hat{x}} \end{bmatrix} = \begin{bmatrix} A_F & -B_FG \\ HC_F & A-BG-HC \end{bmatrix} \begin{bmatrix} x \\ \hat{x} \end{bmatrix}$$

where the subscript F is used to denote the full-order nominal plant, and x denotes the state estimate for the design model. The eigenvalues of the overall closed-loop system using the 3-mode controller are given in Table II. It can be seen from Table II that the overall closed-loop system is stable.

6. CONCLUDING REMARKS

The LQG/LTR multivariable frequency domain technique was employed in the design of an attitude control system for a large flexible space antenna. The LQG/LTR method was noted to be especially attractive for overcoming spillover effects common to large space structures control problem modelled from finite element data. The design objective of avoiding excitation of higher order modes while satisfying performance criteria was met by including these modes in the robustness uncertainity barrier.

Design was based on a reduced order model chosen as the rigid body dynamics plus the fewest number of low frequency vibrational modes necessary to meet a desired closed loop bandwith. Inclusion of the first three vibrational modes (corresponding to the three axes) was found to be necssary to meet a 0.1 rad/sec bandwith. For wider bandwidths, design models width greater than three modes may be needed. A satisfactory control design was obtained using only a colocated single pair of 3-axis attitude sensor and torque actuator for the Hoop/Column antenna problem.

Performance degradation was observed due to the presence of invariant zeros within the design bandwith. These zeros were unavoidable given the prescribed sensor/actuator locations and emphasized the fact that consideration should be given to control aspects when building large space structures.

A modification of the standard LQG/LTR procedure was introduced in which the robustness test was performed with the full LQG compensator

instead of the intermediate Kalman filter design. This approach was found to produce higher gain compensators and helped overcome the basic conservativeness shortcoming of the LQG/LTR approach.

REFERENCES

1. Russel, R. A., Campbell, T. G., and Freeland, R. E.: A Technology Development Program For Large Space Antennas, Paper No IAF-80A33, 31st International Astronautical Congress of International Astronautical Federation, Tokyo, Japan Sept. 21-28, 1980.
2. Sullivan, M. R.: LSST (Hoop/Column) Maypole Antenna Development Program, Parts I and II. NASA CR-3558, June 1982.
3. Balas, M. J.: Trends in Large Space Structure Control Theory: Fondest Hopes, Wildest Dreams. IEEE Trans. Auto. Contr., Vol. AC-27, June 1982.
4. Joshi, S. M.: Control Systems Synthesis for a Large Flexible Space Antenna. Acta Astronautica, Vol. 10, No. 5-6, May 1983.
5. Wang, S. J. and Cameron, J. M.: Dynamics and Control Of A Large Space Antenna. AIAA J. Guidance, Control And Dynamics, Vol. 7, No-1, January-February, 1984, pp 69-76.
6. Kosut, R. L., et al.: Robust Control of Flexible Spacecraft. AIAA J. Guidance, Control and Dynamics, Vol. 6, No. 2, March-April 1983.
7. Doyle, J. C., and Stein, G.: Multivariable Feedback Design: Concepts for a Classical/Modern Synthesis. IEEE Trans. on Auto. Contr., Vol. AC-26, No. 1, Feb. 1981.

8. Stein, G.: LQG-based Multivariable Design: Frequency Domain Interpretation. AGARD Lecture Series LS-117 on "Multivariable Analysis and Design Techniques," 1981.

9. Athans, M.: "Multivariable Control System Design Using the LQG/LTR Methodology". Unpublished lecture notes (lecture given at NASA Langley Research Center, 1984).

10. Chan, S. M., and Athans, M.: Applications of Robustness Theory to Power System Models. IEEE Trans. Auto. Contr., Vol. AC-29, No. 1, Jan. 1984.

11. Kappos, E.: Robust Multivariable Control of the F-100 Engine. MIT Rept. No. LIDS-TH-1328, Sept. 1983.

12. Cruz, J. B., et al.: A Relationship Between Sensitivity and Stability of Multivariable Feedback Systems. IEEE Trans. Auto. Contr., Vol. AC-26, No. 1, Feb. 1981.

13. Armstrong, E. S.: ORACLS - A Design System for Linear Multivariable Control. Marcel & Dekker Control and System Theory Series, Vol. 10, 1980.

LIST OF FIGURES

Table I. Antenna Parameters

Rigid-body parameters

Mass=4544.3 Kg.

Inertia about axes through center of mass ($Kg-m^2$)

$$I_{xx} = 5.724 \times 10^6 \qquad I_{yy} = 5.747 \times 10^6$$

$$I_{zz} = 4.383 \times 10^6$$

$$I_{yz} = I_{xz} = I_{xy} = 0$$

Structural Mode Frequencies (rad/sec)

0.75, 1.35, 1.7, 3.18, 4.53, 5.59, 5.78, 6.84, 7.4, 8.78

Table II. Eigenvalues of the Full Closed-Loop system

Real part	Imaginary Part
$-8.535\ (10^{-3})$	$8.054\ (10^{-2})$
$-8.535\ (10^{-3})$	$-8.054\ (10^{-2})$
$-7.557\ (10^{-2})$	$1.250\ (10^{-1})$
$-7.557\ (10^{-2})$	$-1.250\ (10^{-1})$
$-7.604\ (10^{-2})$	$1.248\ (10^{-1})$
$-7.604\ (10^{-2})$	$-1.248\ (10^{-1})$
$-2.237\ (10^{-1})$	$2.236\ (10^{-1})$
$-2.237\ (10^{-1})$	$-2.236\ (10^{-1})$
$-2.330\ (10^{-1})$	$2.154\ (10^{-1})$
$-2.330\ (10^{-1})$	$-2.154\ (10^{-1})$
$-2.379\ (10^{-1})$	$2.113\ (10^{-1})$
$-2.379\ (10^{-1})$	$-2.113\ (10^{-1})$
$-7.466\ (10^{-3})$	$7.466\ (10^{-1})$
$-7.466\ (10^{-3})$	$-7.466\ (10^{-1})$
$-1.346\ (10^{-2})$	1.346
$-1.346\ (10^{-2})$	-1.346
$-3.076\ (10^{-1})$	1.373
$-3.076\ (10^{-1})$	-1.373
-1.016	1.267
-1.016	-1.267
$-1.702\ (10^{-2})$	1.702
$-1.702\ (10^{-2})$	-1.702
$-4.028\ (10^{-1})$	1.737
$-4.028\ (10^{-1})$	-1.737
$-3.181\ (10^{-2})$	3.181
$-3.181\ (10^{-2})$	-3.181
$-4.422\ (10^{-2})$	4.529
$-4.422\ (10^{-2})$	-4.529
$-5.579\ (10^{-2})$	5.590
$-5.579\ (10^{-2})$	-5.590
$-5.731\ (10^{-2})$	5.776
$-5.731\ (10^{-2})$	-5.776
$-6.685\ (10^{-2})$	6.841
$-6.685\ (10^{-2})$	-6.841
$-6.390\ (10^{-2})$	7.401
$-6.390\ (10^{-2})$	-7.401
$-8.326\ (10^{-2})$	8.782
$-8.326\ (10^{-2})$	-8.782

HOOP/COLUMN ANTENNA CONCEPT

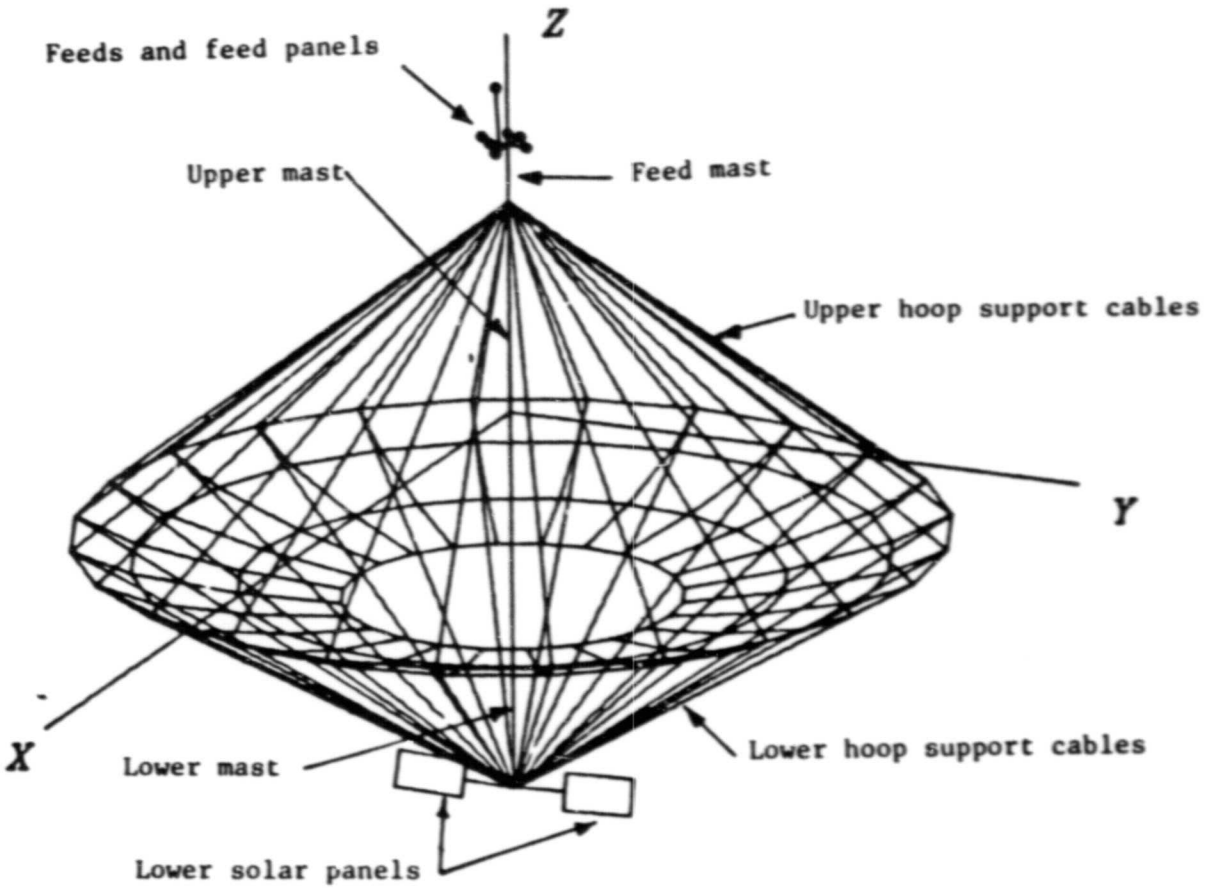

Figure 1.- Hoop/Column antenna concept.

DEFINITION OF UNCERTAINITIES

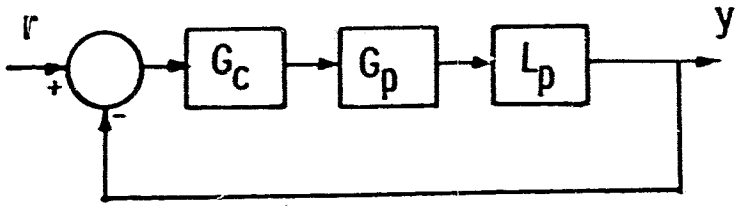

MULTIPLICATIVE UNCERTAINITY

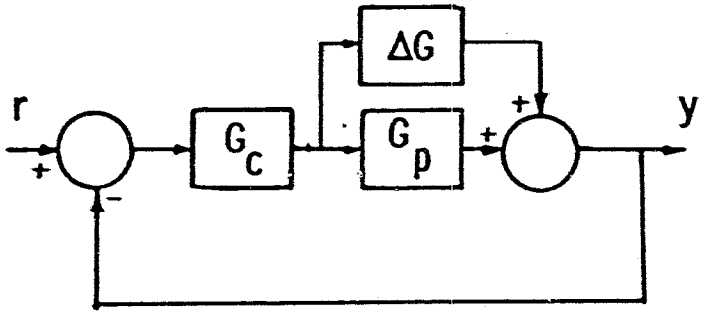

ADDITIVE UNCERTAINITY

Figure 2.- (a) Multiplicative uncertainity

(b) Additive uncertainity.

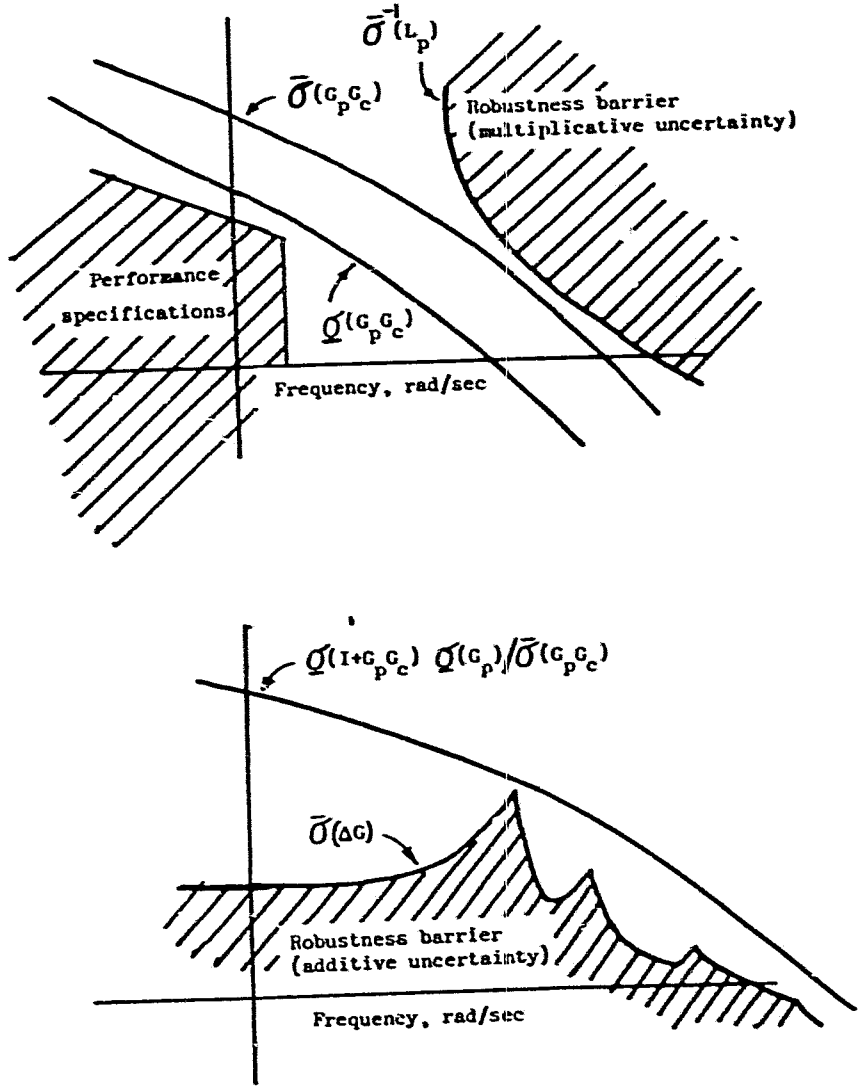

Figure 3.- (a) and (b) Performance and robustness barriers.

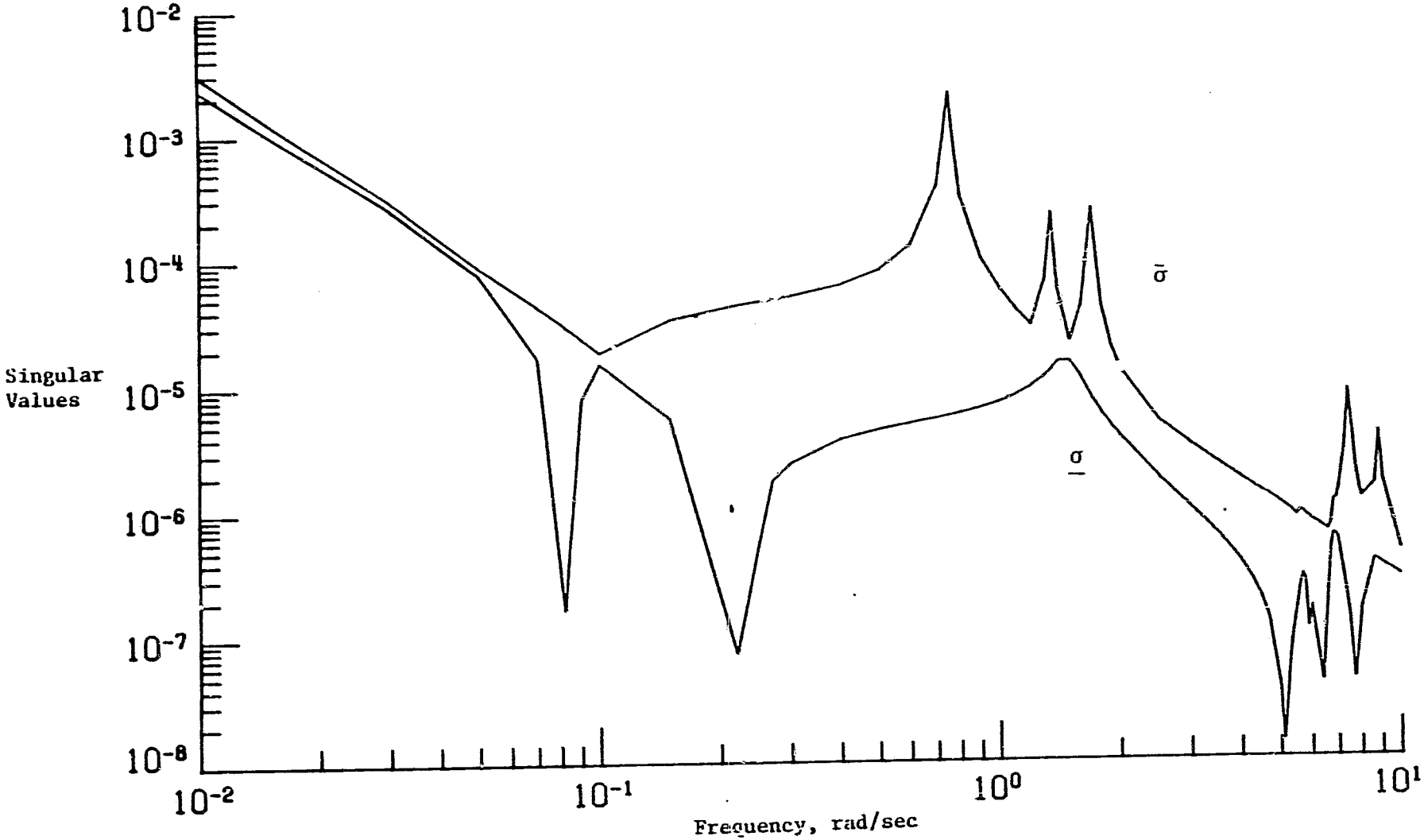

Figure 4.- Singular values of the full nominal plant

STABILITY TEST USING KALMAN FILTER

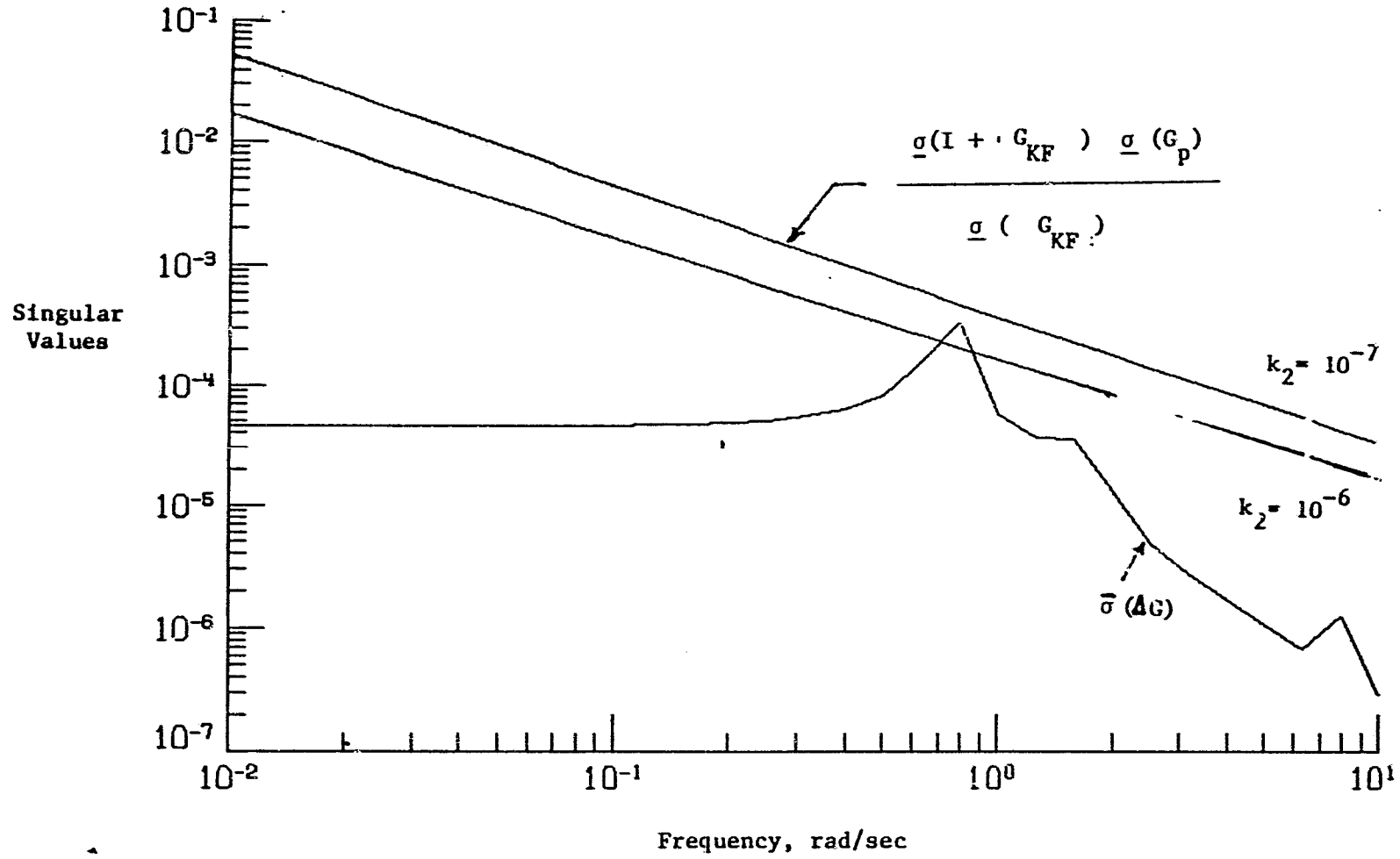

Figure 5.- Stability robustness test (equn.15) for KBF-based loop shaping.

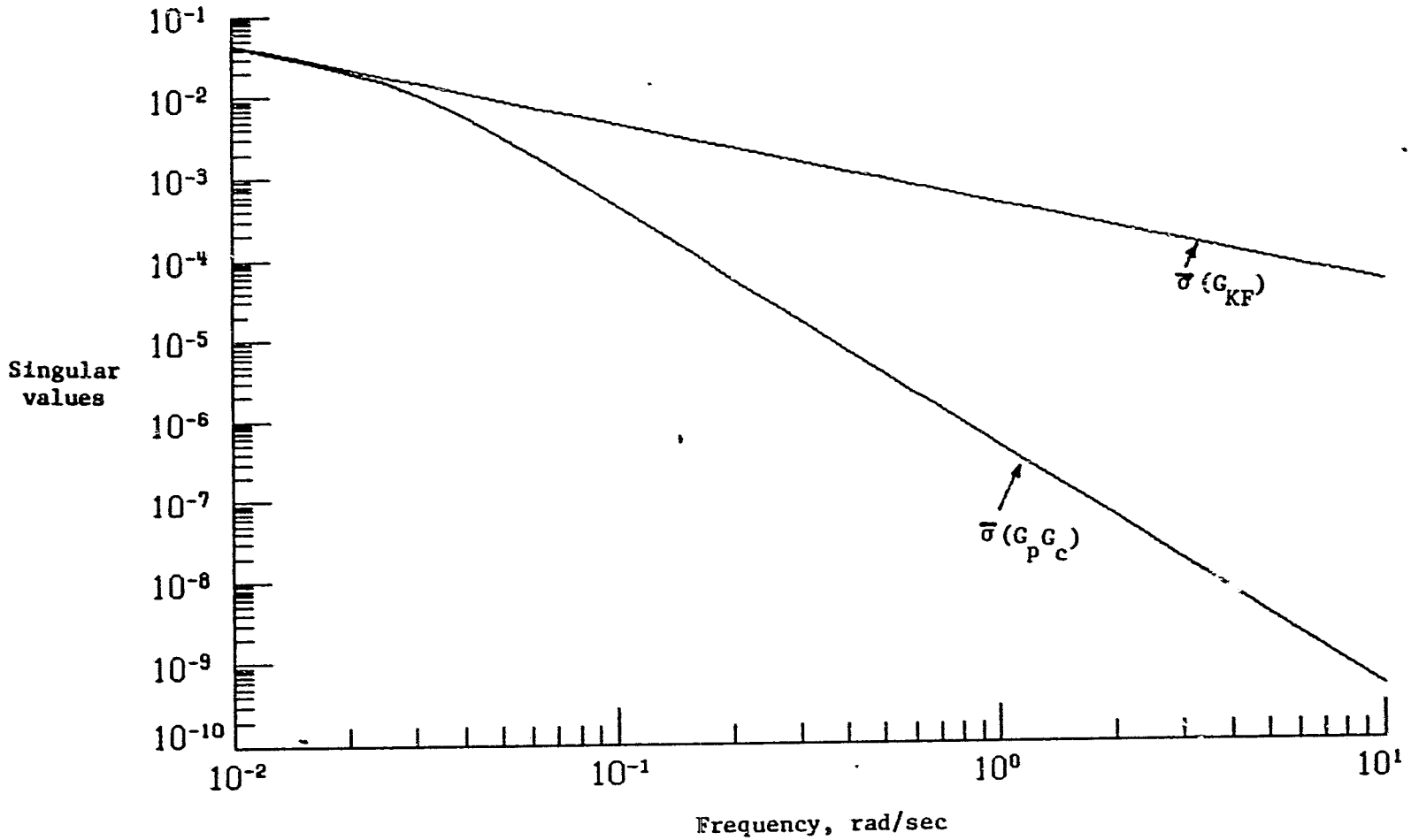

Figure 6.- Singular values of G_{KF} and 'recovered' loop transfer matrix $G_p G_c$

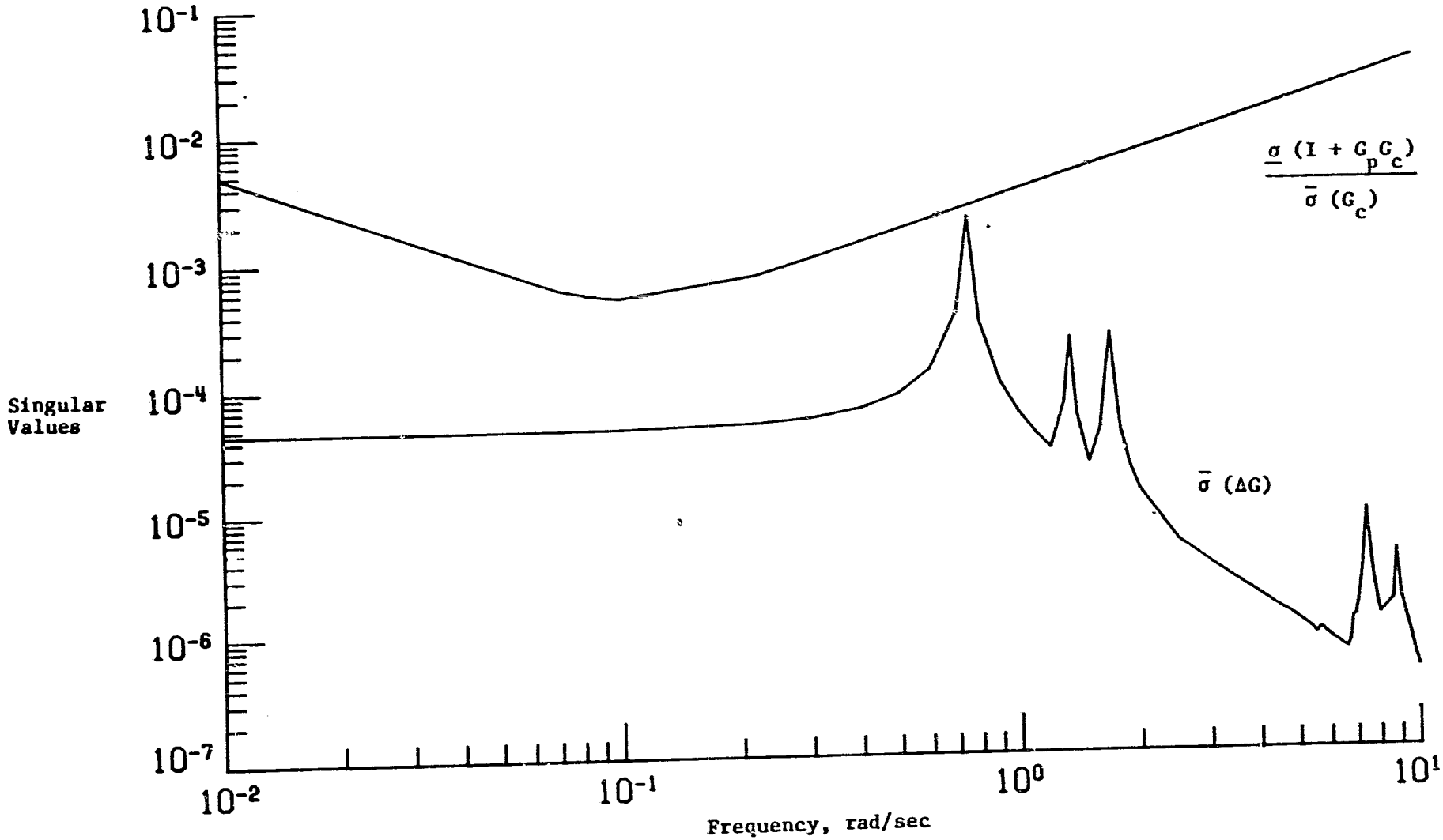

Figure 7.- Stability robustness test (equn. 11) based on the recovered compensator.

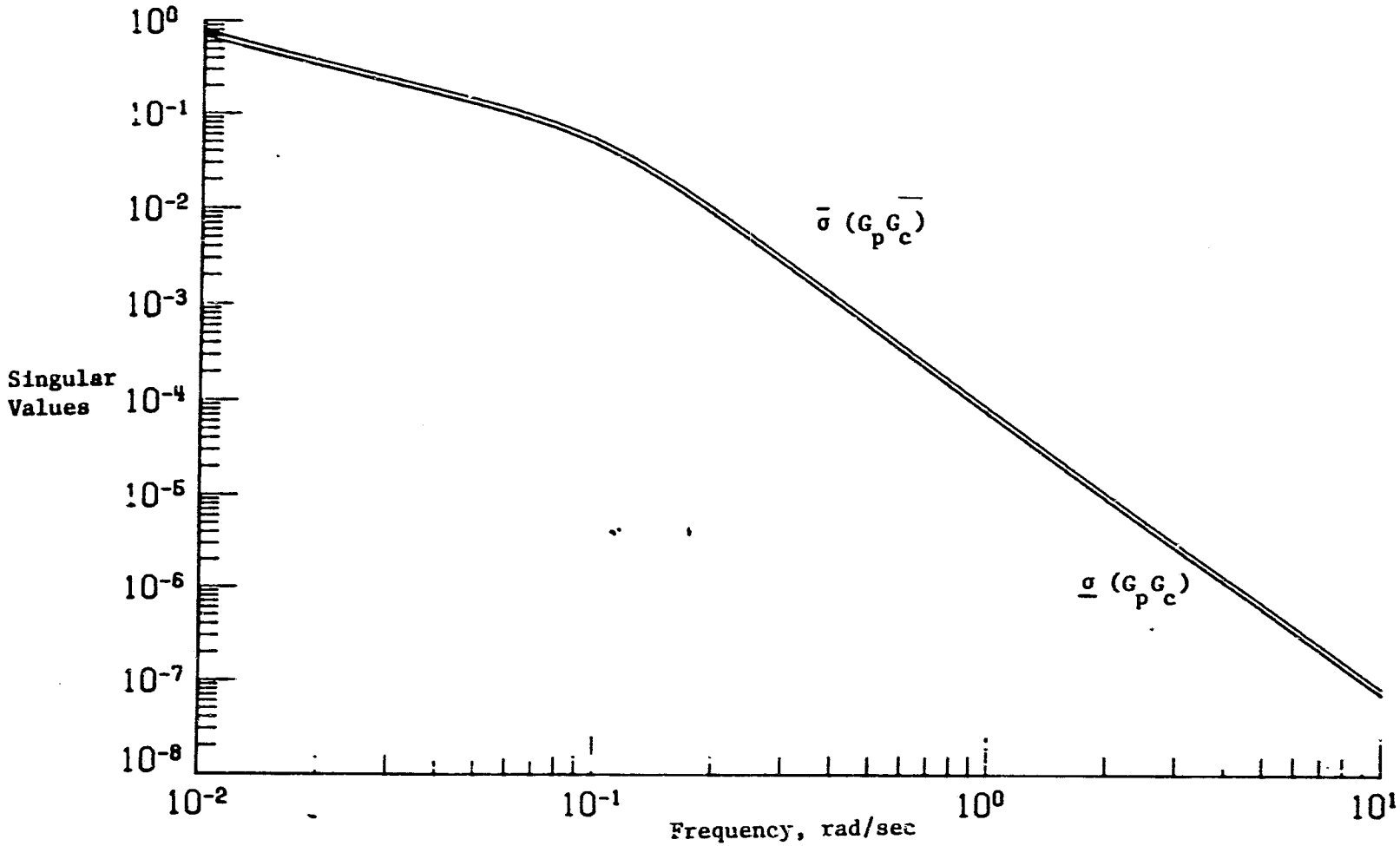

Figure 8.- Singular values of 'recovered' loop transfer matrix G_p G_C

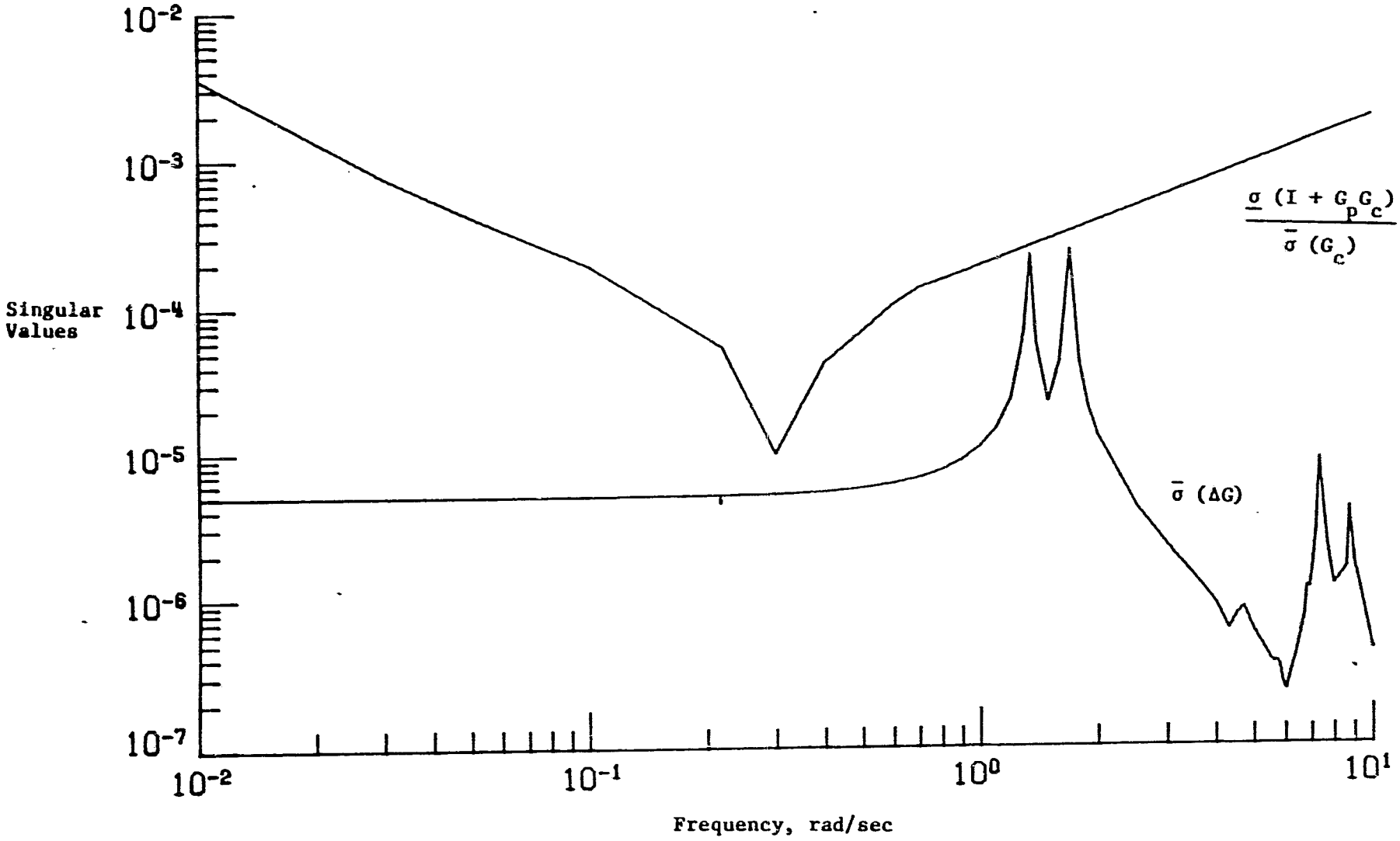

Figure 9.- Stability robustness test for 1 mode model.

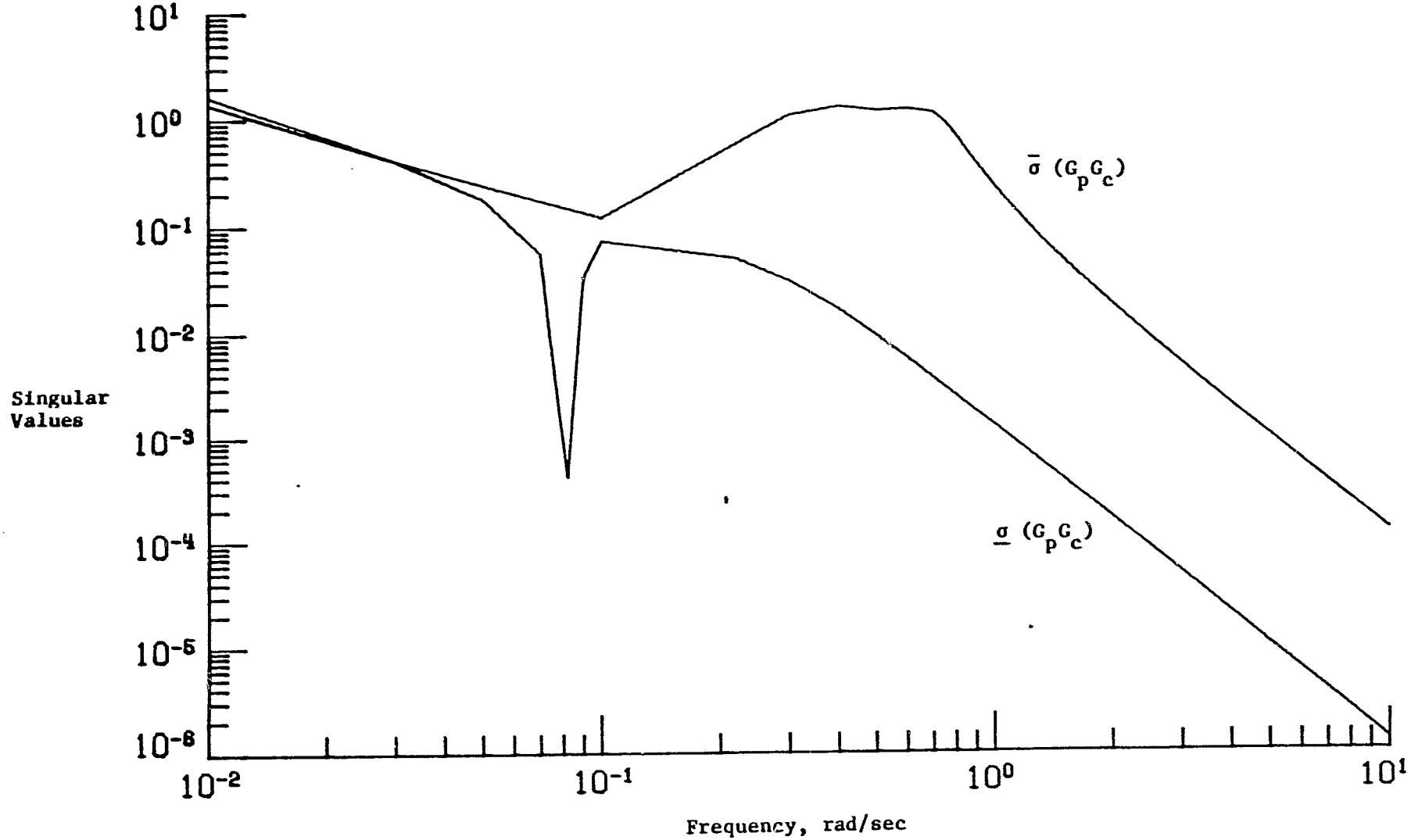

Figure 10.- Singular values of G_pG_C for 1 mode model.

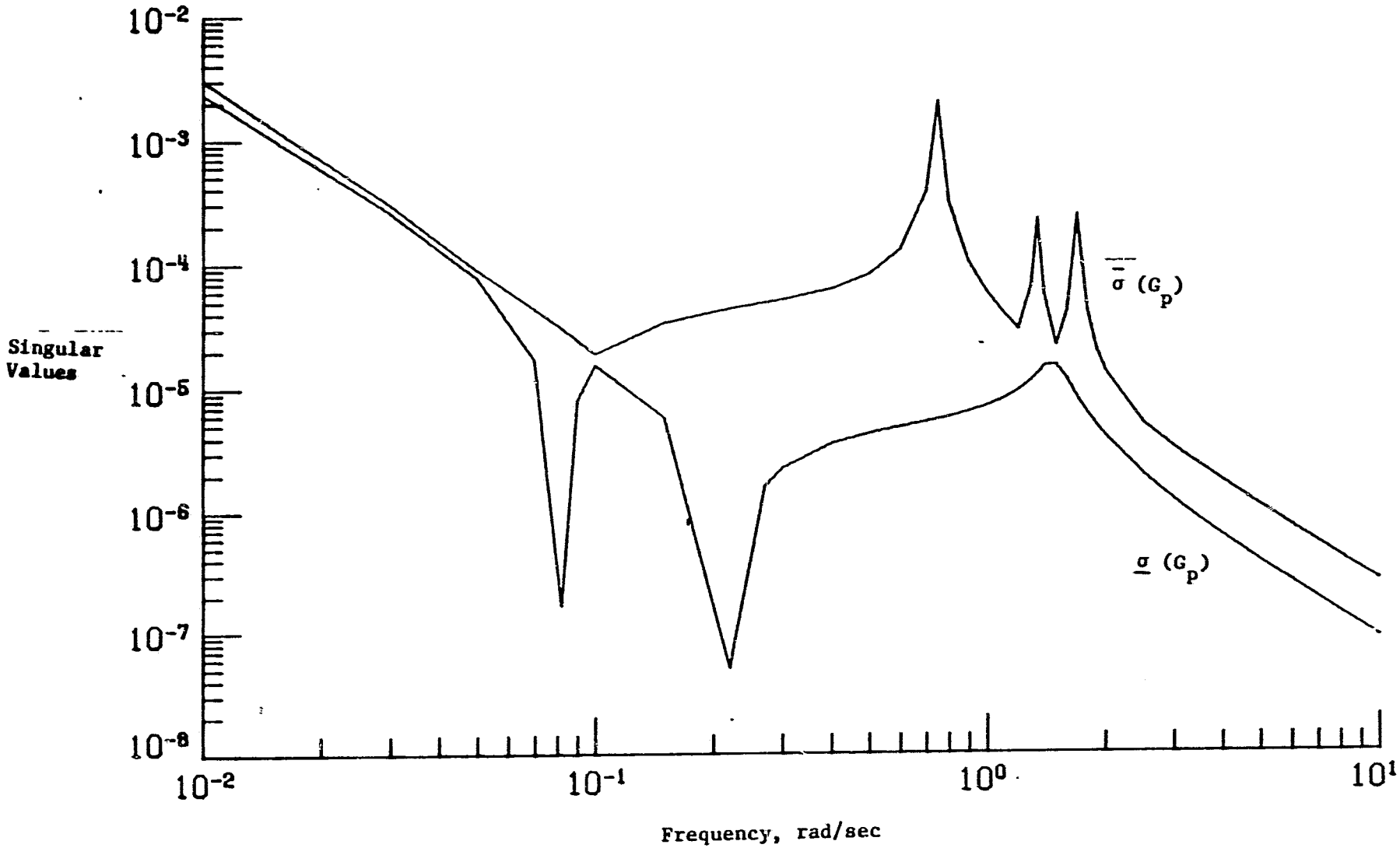

Figure 11. Singular values of G_p for 3 mode model.

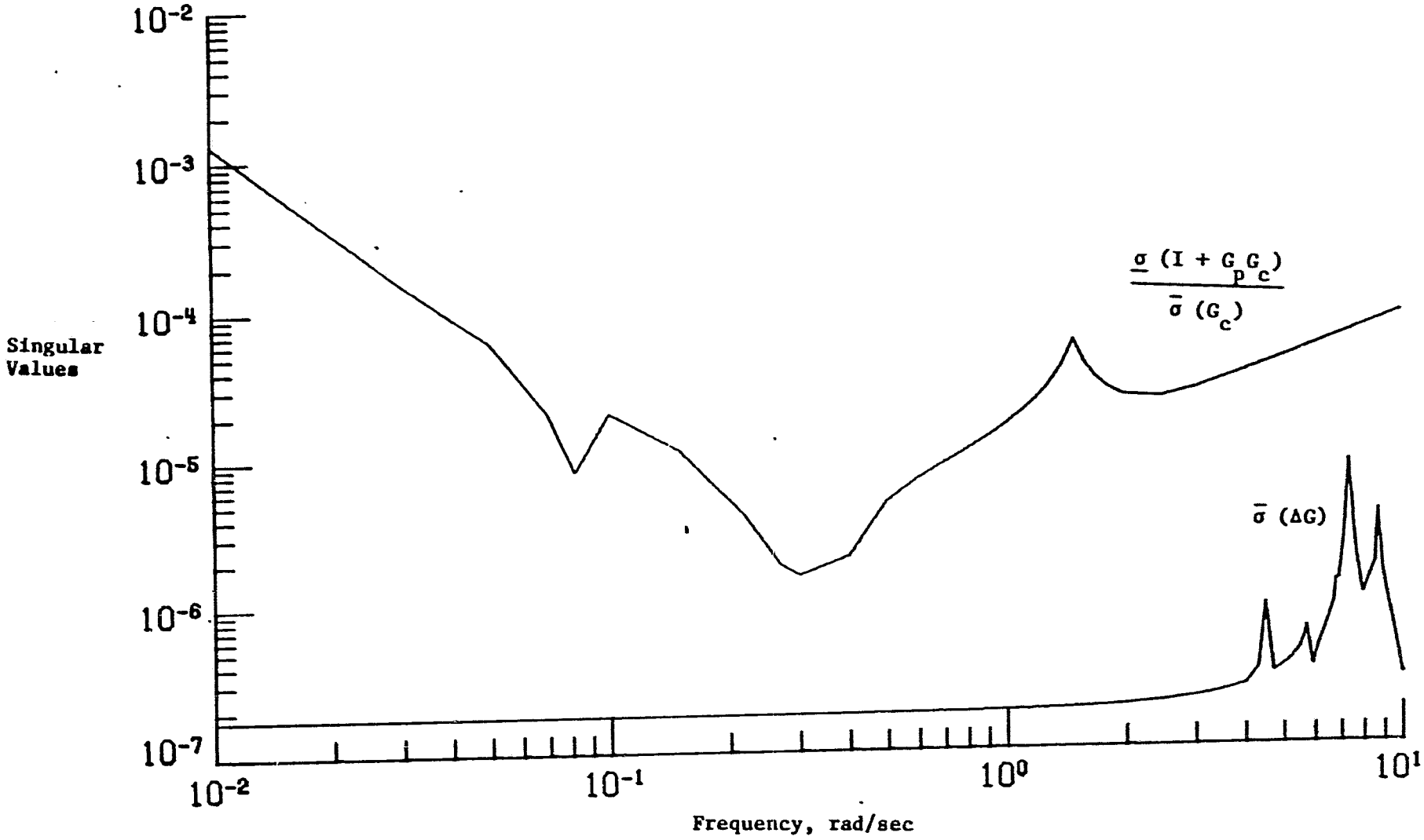

Figure 12. Stability Robustness test (eqn. 11) for 3 mode model.

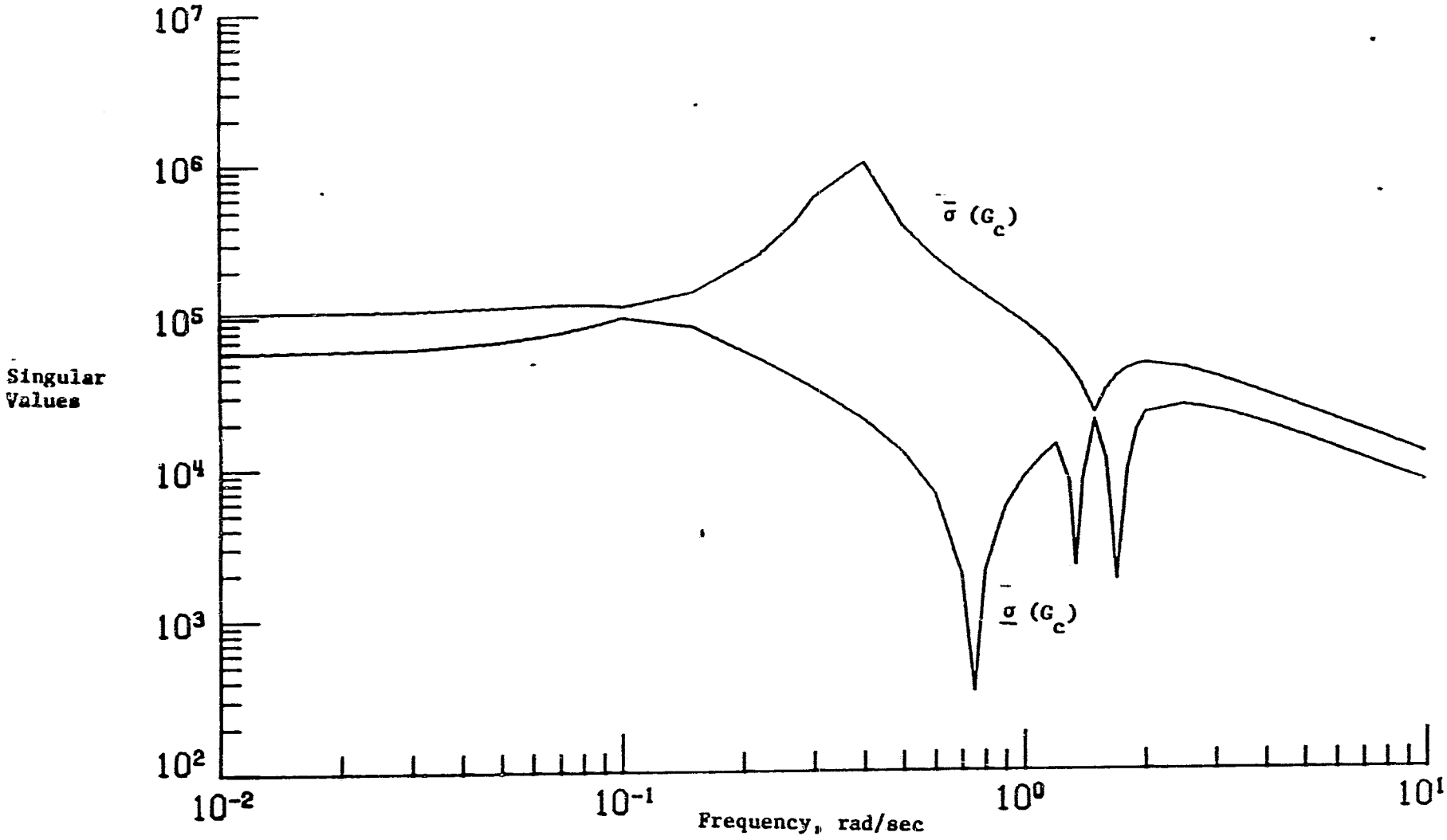

Figure 13. Singular values of the compensator G_c for the 3 mode model.

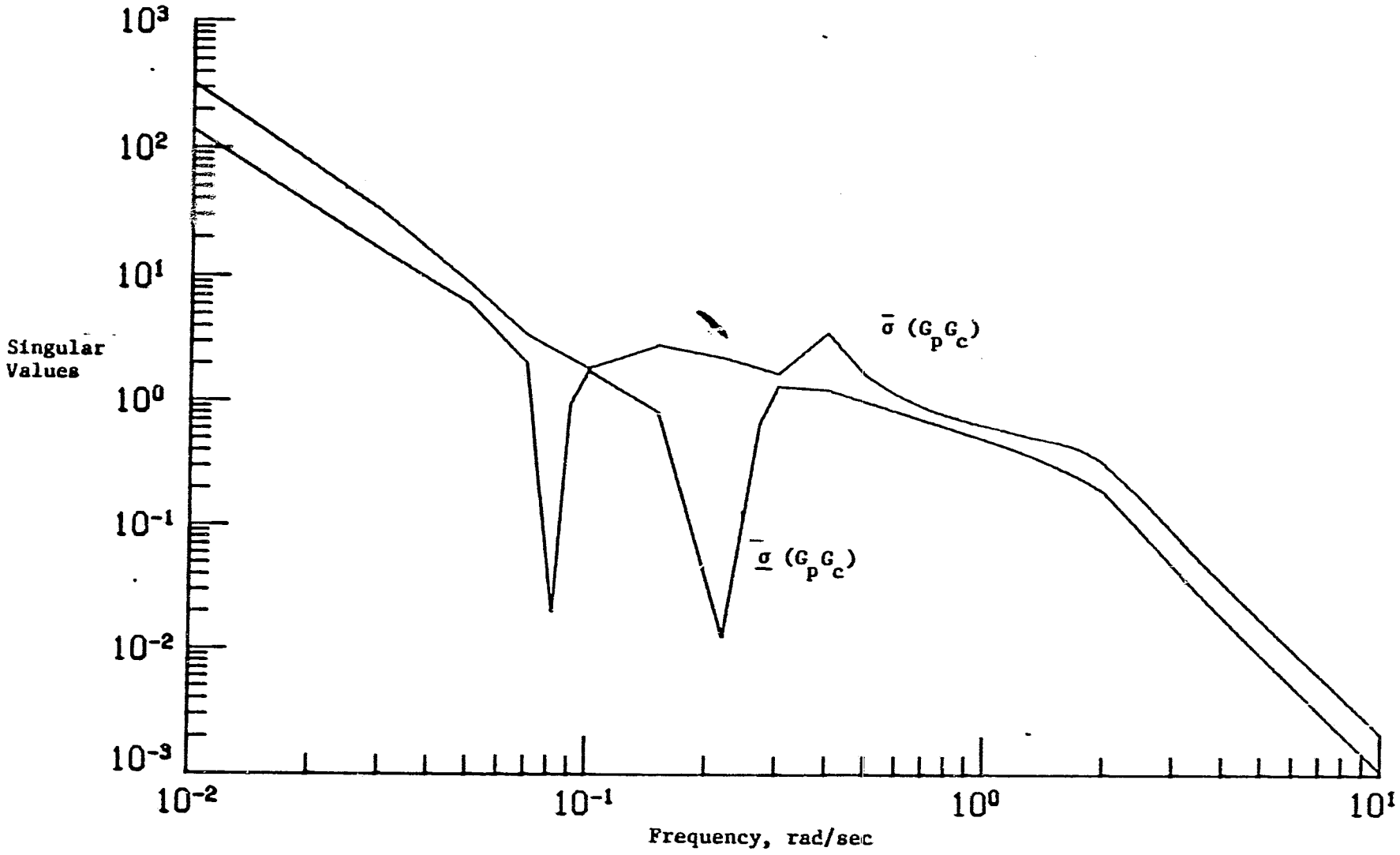

Figure 14. Singular values of G_pG_c ror 3 mode model.